POLYPUBLIE
Polytechnique Montréal

POLYTECHNIQUE MONTRÉAL
UNIVERSITÉ D'INGÉNIERIE

Titre: Title:	Advances in coaxial additive manufacturing and applications
Auteurs: Authors:	Mohammad Rafiee, Floriane Granier, & Daniel Therriault
Date:	2021
Type:	Article de revue / Article
Référence: Citation:	Rafiee, M., Granier, F., & Therriault, D. (2021). Advances in coaxial additive manufacturing and applications. Advanced Materials Technologies, 6(11), 2100356. https://doi.org/10.1002/admt.202100356

⊙ Document en libre accès dans PolyPublie
Open Access document in PolyPublie

URL de PolyPublie: PolyPublie URL:	https://publications.polymtl.ca/10426/
Version:	Version finale avant publication / Accepted version Révisé par les pairs / Refereed
Conditions d'utilisation: Terms of Use:	Tous droits réservés / All rights reserved

📄 Document publié chez l'éditeur officiel
Document issued by the official publisher

Titre de la revue: Journal Title:	Advanced Materials Technologies (vol. 6, no. 11)
Maison d'édition: Publisher:	Wiley
URL officiel: Official URL:	https://doi.org/10.1002/admt.202100356
Mention légale: Legal notice:	

Advances in coaxial additive manufacturing and applications

Mohammad Rafiee*, Floriane Granier, and Daniel Therriault*

Dr. M. Rafiee, F. Granier, and Prof. Dr. D. Therriault

Laboratory for Multiscale Mechanics (LM²), Department of Mechanical Engineering,

Polytechnique Montreal, Montreal, QC H3T 1J4, Canada

Coaxial additive manufacturing (AM) is an emerging technology involving the simultaneous deposition of two or more materials with a common longitudinal axis. It has the potential to overcome the disadvantages associated with conventional single-material AM for the production of core-shell or multi-core-shell multimaterial structures. The coaxial AM techniques can be classified into extrusion and material jetting technologies. The extrusion-based technologies rely on the co-extrusion of multiple materials through a coaxial nozzle whereas the material jetting technologies are based on the introduction of a high voltage electric field between a coaxial nozzle and a grounded collector plate. In this review, we aim to provide a comprehensive overview of multimaterial coaxial AM, including the technologies, nozzle designs, materials and applications. We highlight the advances in coaxial AM and the benefits of this novel technology in various fields. For instance, in biomedicine coaxial AM offers an exciting alternative to single-material bioprinting for the fabrication of bio-scaffolds and vascular networks as well as for tissue engineering and cell encapsulations. Coaxial AM is also a subject of growing interest in the fields of flexible sensors, e-textiles, and printed electronics. We also provide perspectives on the limitations, existing challenges, opportunities, and future directions for further development.

1. Introduction

Multimaterial additive manufacturing involves the fabrication of an object by deposing successive layers on one another using two or more materials [1]. Because it allows the combination of the properties of different materials in a single-step fabrication process, multimaterial AM is starting to change the way of fabricating complex objects in many industries like aerospace, printed electronics, biomedical and e-textile [1]. Among the emerging multimaterial printing approaches, the coaxial additive manufacturing is particularly attractive for different sectors ranging from biomedical and tissue engineering to electronics and continuous fiber-reinforced composites [1,2]. This technology involves the simultaneous deposition of two or more materials with a common axis.

Coaxial AM techniques can be classified into two categories: the extrusion-based technologies, also called "push processes" and material jetting technologies, also known as "pull processes"[3]. Push processes are the most common coaxial AM techniques. They are based on the extrusion of the materials through a nozzle and their deposition in the form of a continuous filament, layer-by-layer to make three-dimensional (3D) objects. Extrusion-based AM technologies can produce accurate shapes at relatively low cost and high geometric complexity with a wide variety of materials such as thermoset and thermoplastic polymers, conductive polymers and bio-inks [1]. So far, silicone [4–9], Polydimethylsiloxane (PDMS) [10,11], and epoxy [4] are the three thermoset polymers reported for coaxial additive manufacturing applications in the literature. On the other hand thermoplastics such as Polylactic Acid (PLA) [12,13], Polycaprolactone (PCL) [13–16] , Polyethylene terephthalate (PET) [17] or Polyvinylidene Fluoride (PVDF) [18] have also been used in coaxial AM applications.

Push processes can further be divided into two main subdivisions: Fused Filament Fabrication (FFF) also called Fused Deposition Modelling (FDM) and the Direct Writing (DIW). In FFF,

heat is normally used to partially melt feed material in a small, portable chamber whereas DIW is based on the extrusion of a liquid-phase "ink" or paste-like material through a nozzle.

Pull processes are based on the use of an extremely powerful electric field that pulls a meniscus and droplets from a pressure-controlled tube to deposit material [3,14].

Coaxial AM offers numerous advantages including the combination of the properties of different materials in a single step fabrication process and the fabrication of hollow structures with often a high geometrical resolution. Moreover, coaxial AM can be used to overcome the limitations of AM regarding certain types of material. For instance, it allows the manufacture of structures made of liquid allows through the use of an enclosing sheath fluid that assures the stability and the continuity of the core material.

Despite the advantages of using coaxial AM to fabricate functioning parts combining the properties of different materials in a single-step process, no comprehensive review has addressed this topic and its many applications. The closest example of a published work is the work of Costantini et al. with review of coaxial 3D printing for biomedical applications [2].

Here, we will initially introduce the coaxial AM technologies based on the material extrusion and the material jetting. Then, in a second section, we will discuss the various design of coaxial nozzles. In a third section, we will explore different promising applications of coaxial AM in different sectors such as biomedical, flexible electronics, or microchannels. Finally, this review will discuss the future development of coaxial AM in design of coaxial nozzles, the improvements of the quality and the functionality of the printed parts and the utilization of coaxial AM to other fields of applications.

The scope of our survey is on coaxial additive manufacturing of structures constituted of multiple distinct materials. Any publication primarily related to internally mixed materials,

continuous fiber-reinforced composites [19,20] or directed energy deposition with coaxial mixing nozzles have been excluded from this review.

2. General background on coaxial AM technologies

Figure 1 shows the two current types of coaxial additive manufacturing technologies groups: extrusion-based and material jetting technologies. In this section, we briefly describe the operating principles and main features of each of these coaxial AM technologies.
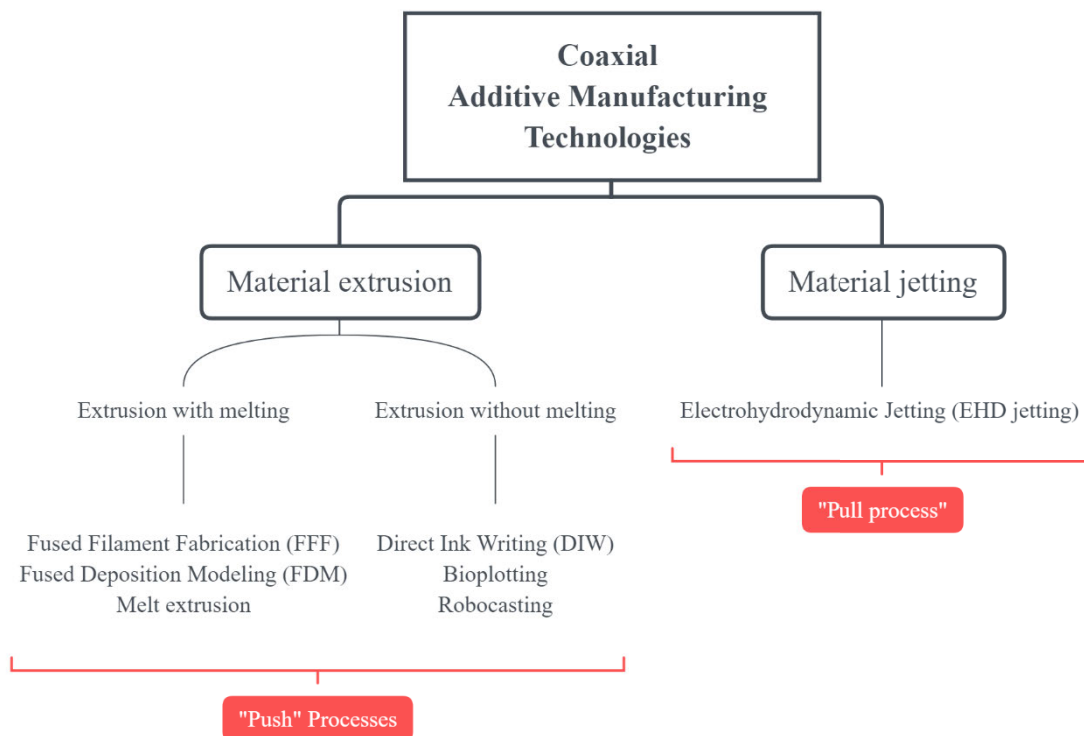

Figure 1. Two classifications of coaxial additive manufacturing: extrusion-based and material jetting technologies.

2.1 Extrusion-based technologies

The popular extrusion-based systems can be classified into two main subgroups as shown in Figure 1: extrusion with or without melting.

Coaxial AM is possible with FFF technology and a schematic of this technique is illustrated in Figure 2. In coaxial FFF, a tractor-feed system pushes two or more materials through the printing head, which generates the extrusion pressure. Heat is usually employed to melt feed materials into chambers as filaments and molten materials are then pushed through coaxial nozzles on a substrate, where they cool down and solidify. The desired coaxial structure is then built layer-by-layer. The materials harden right after flowing from the coaxial nozzles and bond to the layer below.
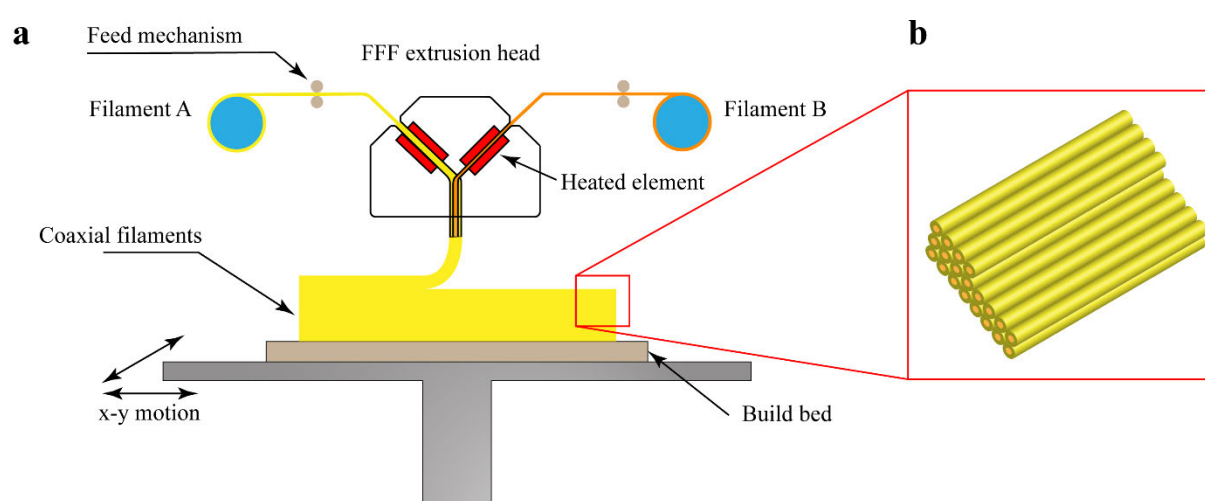

Figure 2. Schematic of a coaxial FFF 3D printer for fabrication of a 3D part with coaxial filaments: **a** a 3D printer with a custom-designed coaxial nozzle, **b** close up view of a multi-layer 3D printed part with coaxial filaments.

Unlike FFF, in extrusion without melting (sometimes also called direct ink writing (DIW), bioprinting or robocasting) paste-like and liquid-like materials called "inks" are used. Figure 3 depicts a schematic of a multimaterial coaxial Direct Ink Writing system. In this process, two or more syringes are filled with different materials. Each syringe is connected to a specific input of a coaxial nozzle and the materials are simultaneously extruded through this nozzle by applying different values of pressure to each syringe.
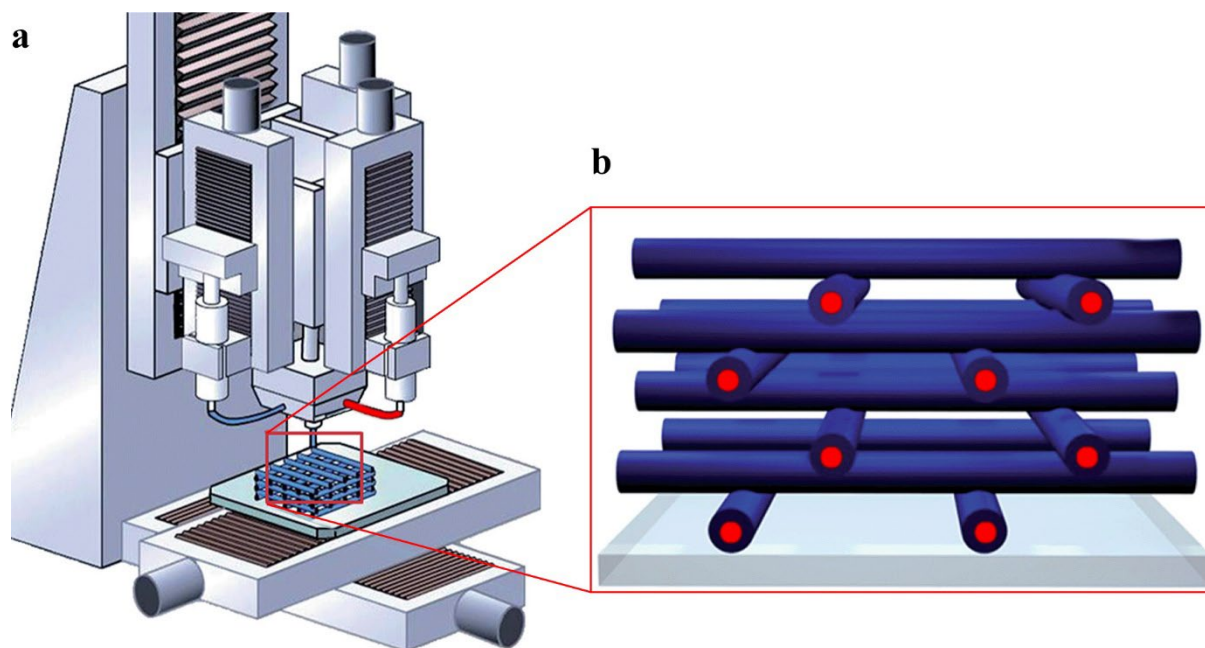
Figure 3. Schematic of a multimaterial coaxial Direct Ink Writing system for fabrication of a scaffold with coaxial struts: **a** robot assisted multimaterial 3D printing system comprised of syringes mounted on independent linear actuators, **b** multi-layer scaffold with multi-core-shell struts. Adapted with permission. [21] Copyright 2014, The Royal Society of Chemistry.

A large number of different ink types can be found in the literature including colloidal inks [22], inks filled with nanoparticle [18], fugitive inks [23], polyelectrolyte inks [24] , and sol–gel inks [25,26]. Once the material is deposited, the ink solidifies due to solvent evaporation, heat energy or other mechanisms.

2.2   Coaxial material jetting

Coaxial additive manufacturing is also possible with material jetting and more precisely electrohydrodynamic jetting (EHD). Coaxial EHD process is illustrated in Figure 4.

Coaxial EHD 3D printing uses a coaxial nozzle made of at least two concentric needles that is connected to at least two syringes filled with different materials. Coaxial EHD combine two

processes: electrospinning and electrospraying that differ from the concentration of the polymer solutions used in these processes.[27] In both processes, a high voltage electric field is applied to pull electrically charged jets out of polymer solutions. But, when the concentration of the solution is high (electrospinning) the jet is stabilized and a continuous flow of material comes out of the nozzle. On the other hand, when the concentration is low (electrospraying), the jet is destabilized and small droplets are formed [3]. Afterwards, in both processes, solvent evaporates to obtain the final structure. Solvent evaporation is a major challenge in coaxial AM. Indeed, this process could be compromised by the presence of the sheath layer, slowing down or blocking the solvent evaporation of the core material.
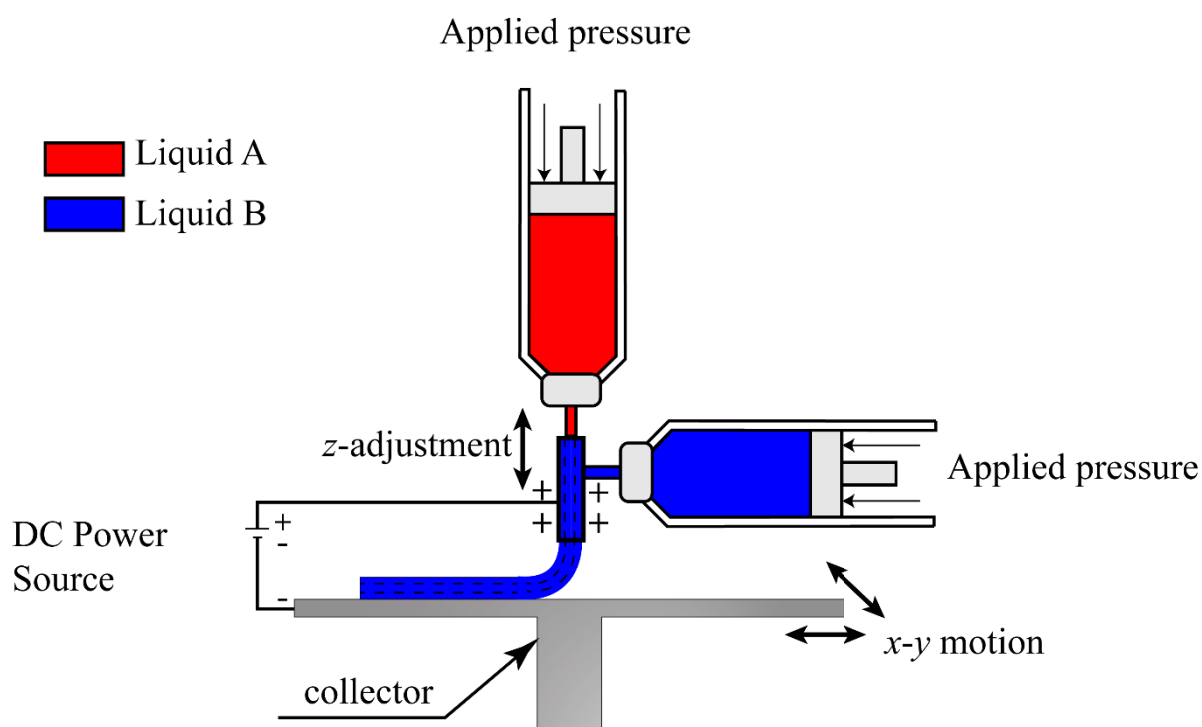
Figure 4. Schematic of coaxial EHD process where a high voltage electric field is used to pull a continuous coaxial flow (or small droplets) from a pressure-controlled capillary tube.

3. Nozzle configurations for coaxial printing and fabrication

Different coaxial nozzle designs and functions for material extrusion and material jetting processes have been elaborated. Table 1 is a summary table of the main characteristics of the nozzle configurations mentioned in this section. Today, the limited printing resolution of coaxial AM systems, the difficulty to ensure a good bonding between the materials as well as the uniformity of the flow of the different materials are key challenges that have to be taken into account in the optimization of the nozzle geometry.

Table 1. Summary table of the characteristics of nozzles described in Section 3.

	Number of nozzles	Size of nozzle (μm)	Material	Manufacturing technique	Applications	Reference
Co-extrusion with melting	1	d_{inner}=300 d_{outer}= 900	Stainless steel	Metal additive manufacturing (selective laser melting (SLM))	Fabrication of different polymer nanocomposites and hydrogel	Figure 5
	1	Nozzle opening = 1 800; Nozzle length = 24 100; Inner needle =22G	Metal alloy (Brass - C36000) Stainless steel	Traditional manufacturing	Stretchable Circuits	Figure 6**a**
	2	d_{inner} = 400 d_{outer} =1200	Titanium alloy (Ti6Al4V)	Metal additive manufacturing (selective laser melting (SLM))	N/A	Figure 9
Co-extrusion without melting	1	d_{outer}= 500	Titanium alloy (6A14V)	Metal additive manufacturing (SLM)	Fabrication of core/shell bioscaffolds	Figure 7**a**
	3	d_{inner1}= 330 d_{inner2}= 406 d_{inner3}=508 d_{outer}=1600	N/A	Traditional manufacturing	Fabrication of hollow calcium alginate filaments	Figure 7**b**
	2	N/A	N/A	Traditional manufacturing	Construction of Blood Vessels	Figure 7**c**
	1	N/A	Stainless steel for the needles, Quartz	Traditional manufacturing	Fabrication of alginate hollow fibers	Figure 7**d**
	1	d_{inner} = 260 d_{outer} = 690	Stainless steel needles, Silicone glue for fixation	Hand-assembled	Prototyping of chitosan-coated alginate scaffolds	Figure 7**e**
	3	d_{inner1}= 1010 d_{outer2}= 2000 d_{inner2}= 630 d_{outer2}= 1250 d_{inner3}=260 d_{outer3}= 500	Resin (PR48)	Additive manufacturing (SLA)	Fabrication of hollow tubes	Figure 8**a**
	1	d_{inner}= 100	Resin (Asiga plastclear) and stainless-steel needle	Additive manufacturing (digital light processing)	Various biological applications (hollow hydrogel spheres, encapsulating cells ...)	Figure 8**b-c**

3.1 For melt extrusion

Figure 5**a** shows the multimaterial coaxial extrusion system, including a coaxial extrusion

nozzle and dual material reservoirs designed by R. Cornock [13,15,16]. Their custom-made coaxial

nozzle contains two separate chambers for the material inputs, with independent temperature and pressure controls, oriented at 60° with respect to the extrusion direction and aligning at the extrusion tip (

Figure 5**b**(i-ii)). The authors simulated the flow behavior within the nozzle in order to optimize its design using the FloExpress extension of Dassault Systemes Solidworks 2012 (

Figure 5**b**(iii)). The metal additive manufacturing method called selective laser melting (SLM) was used in the manufacturing of the stainless steel 316 L coaxial melt extrusion nozzle, with diameters of $300\mu m$ and $900\mu m$ for the inner and outer nozzles, respectively (

Figure 5**c**). The inner nozzle is 200 μm longer than the outer one as shown in

Figure 5**c**(iii). After removing the supporting material, electropolishing was performed to smooth the surface of the additively manufactured coaxial nozzle. Their coaxial nozzle can be potentially used for the manufacture of different polymer nanocomposites and hydrogel materials since each chamber has its own temperature and pressure control systems.

Khondoker et al. [28,29] developed a custom-made thermoplastic tri-extruder compatible with FFF printers (see Figure 6**a**). The printing head has two angled input channels made of a metal alloy (brass - C36000) for feeding thermoplastic materials and a third one in the middle, made of a reusable stainless-steel dispensing needle (22G) assigned to the extrusion of a central fluid core. The nozzle formed has an opening of 1.8mm.

Ragones et al. [30] used a special extrusion nozzle made of three to five input channels (see Figure 6**b**), compatible with FFF printers, for the manufacture of multi core-shell structures. With this device, they were able to simultaneously co-extrude up to five different materials and build complex objects such as a flexible multi-coaxial-cable-type battery in a single-step process.
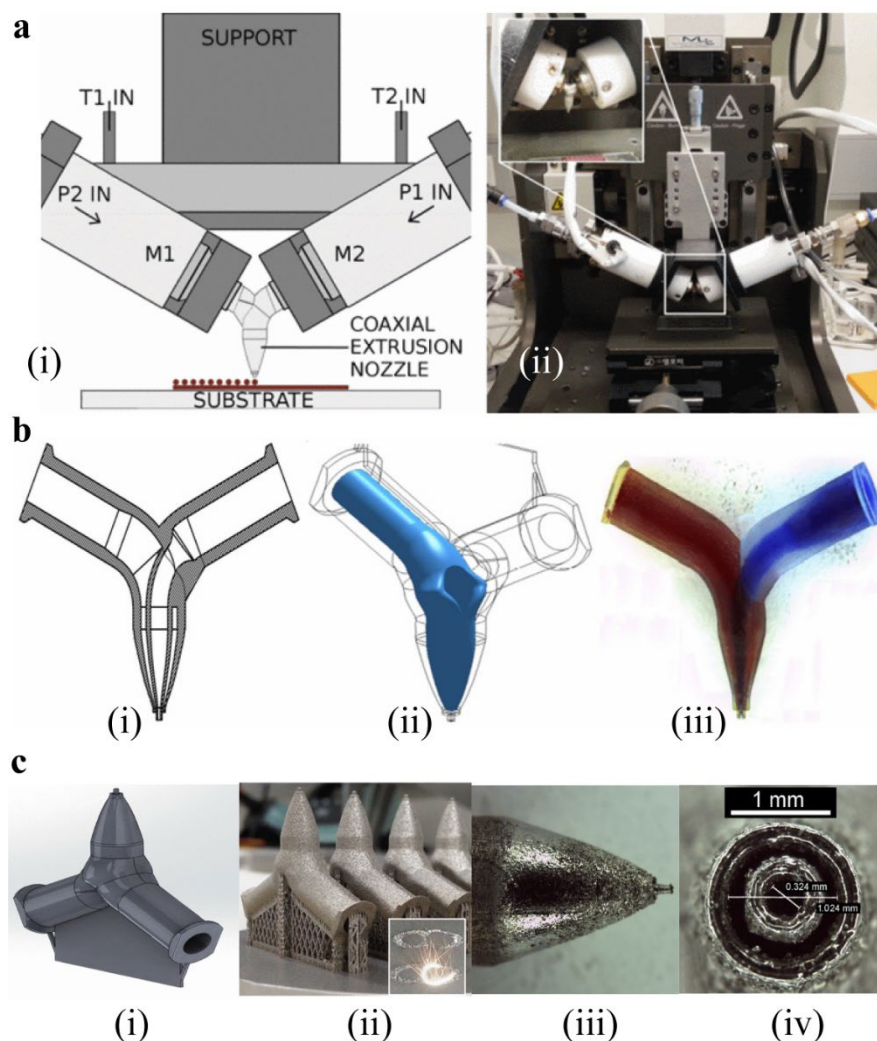
Figure 5. **a** (i) Schematic and (ii) picture of a multimaterial coaxial extrusion system, including a coaxial extrusion nozzle and dual material reservoirs, with independent temperature and pressure controls. Adapted with permission. [15] Copyright 2013, IEEE; **b** Coaxial FFF nozzle design: (i) 2D section drawing (ii) example of flow analysis using FloExpress extension for Solidworks ; (iii) 3D printed prototype using transparent material. 2% Alginate hydrogel solution with methyl red (left) and brilliant blue (right) are loaded into the separate chambers to show the internal architecture of the component; Adapted with permission. [16] Copyright 2014, IOP Publishing: **c** (i) Solidworks CAD model of the coaxial nozzle. Adapted with permission. [15] Copyright 2013, IEEE; (ii) SLM 3D printed coaxial extrusion nozzles. Adapted with permission. [15] Copyright 2013, IEEE; (iii) optical

microscopy image of the coaxial extrusion nozzle tip following 120 s electropolishing at 5.0 V. Adapted with permission. [16] Copyright 2014, IOP Publishing; (iv) optical microscopy image of coaxial nozzle cross-section at the tip, designed at 300 μm/900 μm. Adapted with permission. [16] Copyright 2014, IOP Publishing.
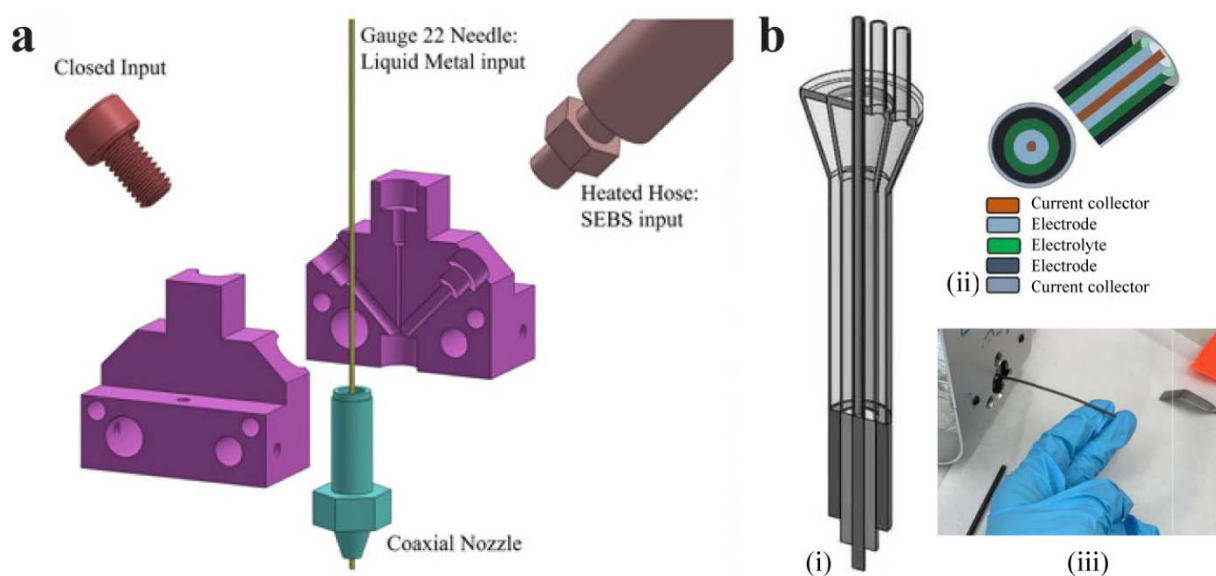

Figure 6. Two custom made melt extrusion coaxial nozzles: **a** an exploded 3D model of a tri-extruder used for coaxial extrusion of liquid metal with a thermoplastic shell. Adapted with permission. [28] Copyright 2019, John Wiley and Sons; **b** (i) cross-sectional view of an extrusion nozzle for fabrication of multi-coaxial (multi-core-shell) cable battery, (ii) schematic design of the multi-coaxial battery; possible configurations of printed flexible multi-axial cable battery, (iii) optical image of a cathode filament extrusion. Adapted with permission. [30] Copyright 2019, IOP Publishing

3.2   For DIW and EHD jetting

A great number of nozzles with various shapes and functions were designed for both DIW and EHD jetting processes. Some of these nozzles are illustrated in Figure 7. Figure 7**a** shows a custom-made dual concentric coaxial nozzle with the capability to be embedded in a handheld device designed to perform in situ surgical cartilage repair. This nozzle was used by Duchi et al. [31,32] to 3D print core/shell bioscaffolds. The dual concentric coaxial nozzle has two parallel connectors that were attached to two cartridges filled either with the core or the shell solution making the printing device more compact than the angled-channels designs mentioned before. This nozzle enabled the two compartments to be dispensed with a maximum resolution of 500 μm. Gao et al. [33] developed a different coaxial bioprinting nozzle as depicted in Figure 7**b**. The nozzle was made of seven deferent parts (see Figure 7**b**(ii)): an inner tube, an outer tube, two feed tubes, a storage tube, a sealed cap, and a porous buckle, and its two connectors were perpendicular to one another. The outer tube was made of a 14.5G needle whereas three types of inner needles featuring a needle nominal internal diameter of size of 0.514, 0.413 and 0.337 were used in this coaxial device.

 Similar to nozzle described in Figure 7a, an alternative nozzle was designed by Liu et al. [34] that features a pressure control system and a temperature control system (see Figure 7**c**). The pressure control system allows the control of the material distribution at different speeds by adjusting the pressure in each cavity. The temperature control system ensures a constant temperature for thermosensitive materials (e.g., 37°C) and the solidification of the material at low temperature (e.g. 4°C).

Figure 7**d** depicts a custom-made coaxial spinneret developed by Li et al. [35] that was used to print gelatin-alginate hollow fibers. This spinneret was made of four different parts represented in Figure 7**d**(ii): an inner nozzle, an outer nozzle that was 5 mm shorter than the inner one, a T-

fitting and a quartz tube use to make the outer needle as long as the inner one, forming a tube-shaped reactor. The design presented some advantages including easy and inexpensive manufacturing, and easy cleaning of clogged nozzles since it was made of several removable parts.
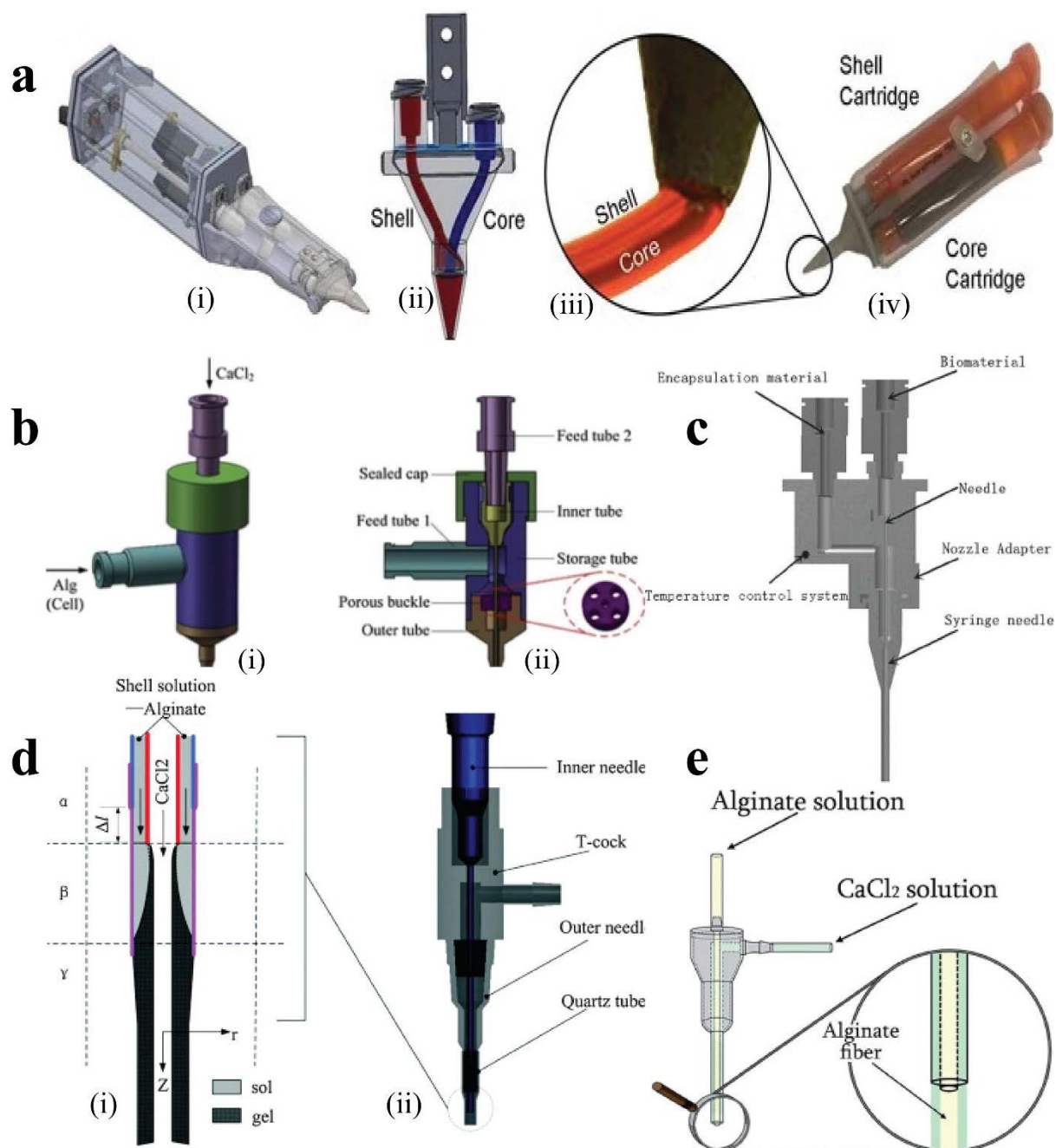

Figure 7. Coaxial nozzles: **a** (i) schematic representation of a 3D co-axial handheld printer, (ii) schematic representation of the co-axial nozzle, (iii-iv) optical picture of the cartridges

dedicated to core and shell loading in the printer, with magnification. Adapted with permission. [31] Copyright 2017, Nature Springer; **b** (i) 3D model of a coaxial nozzle for bioprinting with built-in microchannels for nutrients delivery; (ii) cross-sectional view of the coaxial nozzle assembly mode. Reproduced with permission. [33] Copyright 2015, Elsevier; **c** cross-sectional view of a coaxial nozzle with temperature control capability for construction of blood vessels. Reproduced with permission. [34] Copyright 2017, Society for Laboratory Automation and Screening; **d** schematic of a 3D printed hollow hydrogel fiber and the scaffold. (i) CaCl2-in-alginate coaxial microfluidic; (ii) reactor-like spinneret. Adapted with permission. [35] Copyright 2016, Royal Society of Chemistry; **e** schematic representation of a coaxial needle for the extrusion of alginate fibers. Adapted with permission. [36] Copyright 2014, Royal Society of Chemistry.

The nozzle represented in Figure 7**e** was fabricated in a more rapid, easy and inexpensive way. Colosi et al. [36] used two needles, featuring a gauge size of 26G and 19G, assembled inside one another and fixed with silicone glue.

Millik et al. [37] designed and 3D printed custom-made coaxial nozzles using the Autodesk Ember DLP 3D printer and the Autodesk Standard Clear Prototyping Resin (Figure 8**a-b**). They made several nozzles of different geometrical parameters. Millik et al. used the same printing parameters to manufacture each of these nozzles: the layer height was set to 50 μm, no support was used and nozzles were fabricated so that their top surfaces were in contact with the printing bed. Post-printing processes included the use of isopropanol to rince the parts, the purge and drying of the nozzles using pressurized air and a post-curing step. Afterwards, blunt-tip needles were fixed to the different inlets of each coaxial nozzle. Schematics of these 3D-printed nozzles and the setup used to manufacture coaxial hydrogel tubes are shown in Figure 8a.
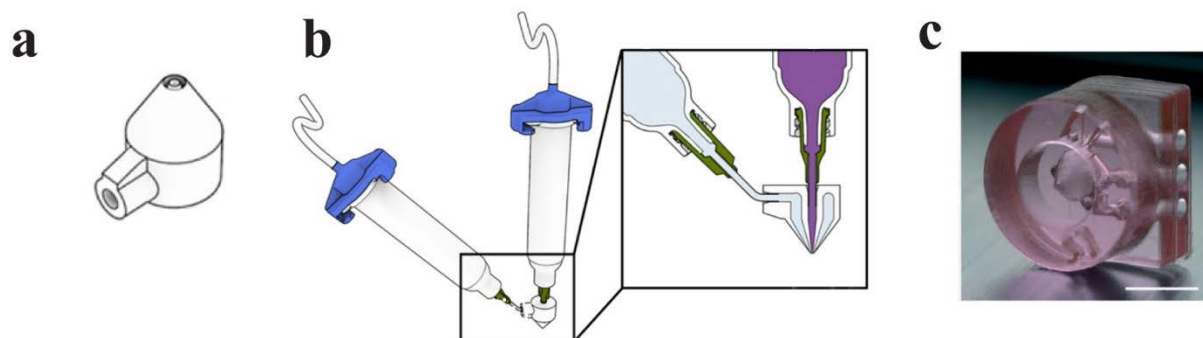
Figure 8. 3D printed custom-made coaxial nozzles: **a**(i) schematic of SLA 3D printed coaxial nozzle, (ii) schematic of the interior of the coaxial nozzle used to print hydrogel tubes. Adapted with permission.[37] Copyright 2019, IOP Publishing Ltd, **b** close-up picture of the coaxial nozzle (scale bar 500 µm). Adapted with permission. [38] Copyright 2016, Royal Society of Chemistry

Alessandri et al. [38] also chose to design their own coaxial device (Figure 8**c**). In their work, the coaxial nozzle which was a microfluidic device was 3D printed with a digital light processing (DLP) 3D printer using Asiga plastclear resin. The print was then rinsed with ethanol and later cured for 30 to 60 minutes. Three 19G stainless steel tubes of 1 cm long were then attached to the inlets with epoxy resin. This setup presented a high versatility, allowing its use in many biological applications.

4. Modeling of coaxial AM

Since coaxial AM is a new and innovative technology, researchers make great use of numerical simulation to optimize the printing features and predict the behavior of the fabricated coaxial structures.

4.1. Design optimization of coaxial nozzles

Numerical simulation can be a powerful tool to predict the performance of the coaxial nozzle, in terms of material flow stability and continuity within the different channels, before its fabrication. For instance, Taylor et al.[13] conducted a study in order to determine the optimal design for the coaxial nozzle they used in the coaxial FFF system. Using Solidworks, they designed several nozzles as the ones depicted in Figure 9**a** differing only in the geometry of the external fluid pathway. Then, the authors used ANSYS CFX to perform thermal and flow simulations on the different 3D models and selected the design allowing a more uniform distribution of the fluid velocity within the nozzle. The results of the simulations showing the fluid velocity distribution within each of the two nozzle designs are represented in Figure 9**b**. In some cases, such as the one illustrated in Figure 9**b**(i), the simulation predicts the appearance of a velocity imbalance within the external fluid pathway. Thus, out of the two nozzle designs depicted in Figure 9, the authors selected the second one based on the results of their simulations.
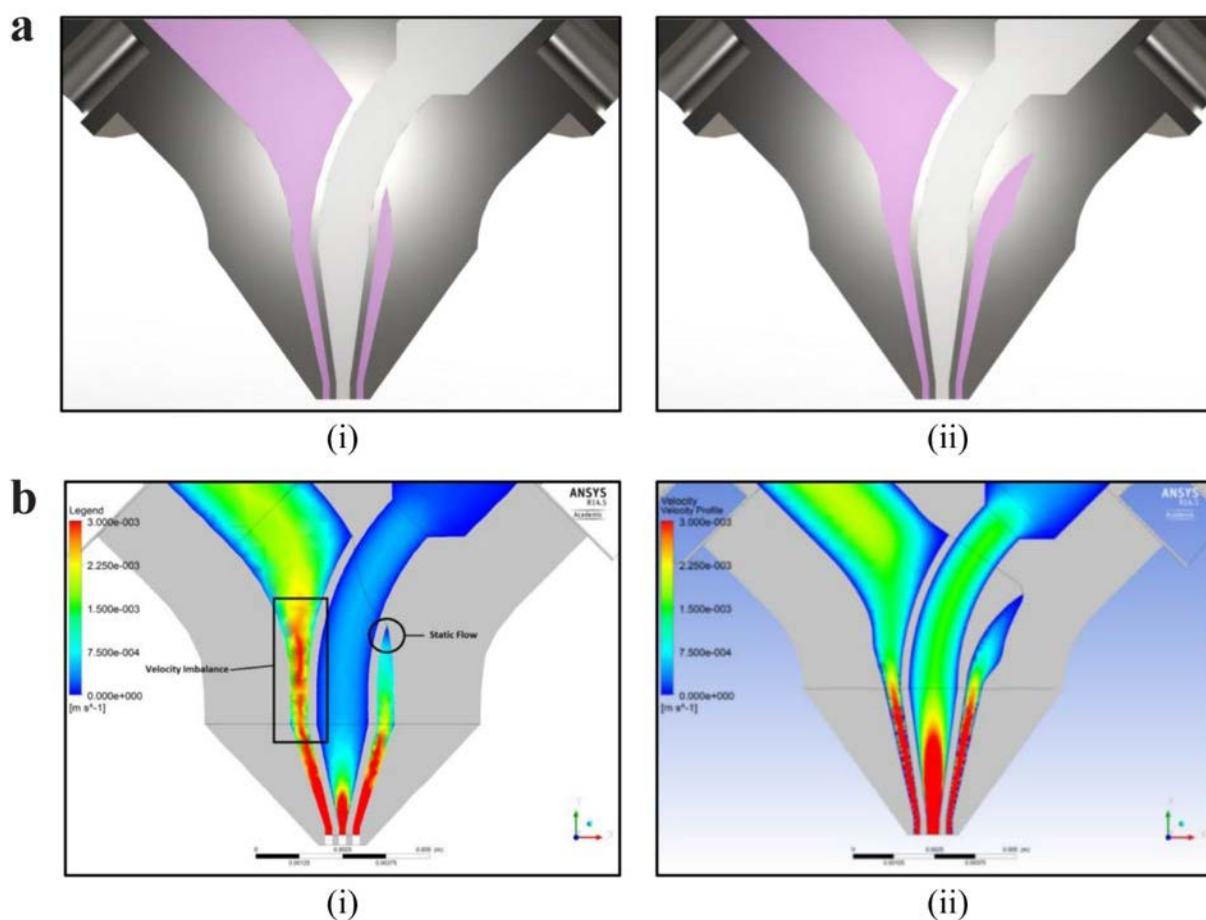
Figure 9. Graphical representation of a Solidworks models of two coaxial nozzle designs differing in the geometry of the external fluid pathway: (i) straight external fluid pathway, (ii) 5° oriented external fluid pathway; b (i-ii) computational fluid dynamics. Adapted with permission. [13] Copyright 2017, Emerald Publishing Limited.

Jin et al.[39] studied the feasibility of coaxial fabrication of doubled-layer (core–shell–shell) capsules in a vibration-assisted dripping process. The authors designed a three-layered coaxial nozzle and carried a simulation, using ANSYS, of the fluid velocity distribution within the annular and the sheath channel of the nozzle in order to optimize the design before manufacturing the device. The geometrical parameters of the nozzle were chosen to make the velocity distribution uniform within the nozzle and at its outlet.

Silva et al.[40] also used a computationally aided design model to analyze three triple-layered coaxial nozzle designs differing from the diameter of each of the three channels ($d_{inner}/d_{middle}/d_{outer}$= 23G (Gauge)/18G/14G; 25G/18G/14G; 20G/15G/13G) in order to optimize the cell viability in biofabrication applications. Using COMSOL Multiphysics, the authors performed simulations to determine the fluid velocity and the pressure distribution within each of the channel of the nozzle. In the end, all three proposed nozzle designs proved to be suitable for bioprinting with bioinks with similar composition or rheological properties to the materials used in their study. Indeed, a cell viability above 80% in alginate-based hydrogels was guaranteed using each of the nozzle when the extrusion pressure was kept below 34 kPa.

4.2. Simulation of the properties of the coaxially printed structures

Simulations are not only useful to simulate the velocity and pressure profiles, but also are used to predict the interaction of the materials after deposition. For instance, Li et al.[35] modelled the morphological evolution of the alginate hollow fibers 3D printed using a reactor-like spinneret. Thanks to the rotational symmetry of the object, they were able to minimize the difficulty of the problem by considering a simplified axisymmetric 2D problems (the fibers were considered as rectangles and not cylinders). The simulation was based on the resolution of the Navier Stokes, the gelation reaction and the shrinkage profile equations. The results of the simulation were then compared to on-line observations of extrusion states for validation.

Xu et al.[41] printed smart elastomeric foam and used coaxial AM to embed piezo-resistive sensors within the structure. One of the major challenges of 3D printed smart cellular materials is improving their mechanical properties. The authors performed a finite element analysis, using ABAQUS, to determine the mechanical properties of the two types of printed structures: simple cubic (SC) and face centered tetragonal (FCT) foams. A shell diameter of 1.30 mm, a spacing between the lines of 3 mm and a layer height of 1.1 mm were chosen as parameters for the

simulation. Moreover, Xu et al. considered that the structure was sandwiched between two high stiffness plates and the simulation consisted of applying a linear displacement to the top plates to compress the structure. The maximum strain was fixed at 0.5. The simulation results showed that, within the FCT foam, the struts experienced a dominant stretching provided by compressing the staggered strands adjacent to the strain sensor whereas in the SC, the dominant stretching was located where the upper and lower struts were vertically aligned. The von Mises stress measured in the FCT foam was higher than the one in the SC one for a given strain. These predictions were confirmed by experimental tests and based on these results, FCT structure featuring a higher sensitivity was chosen as the optimum cellular design in the rest of the study.

5. Applications of coaxial 3D printed structures

There are many coaxial AM applications (see Figure 10) including vascular networks, tissues and organs, and fluidic and microfluidic devices for biomedical industry, mechanical reinforcements, sensors and actuators, and batteries for aerospace and energy sectors. In this section, we will take a look at some of these applications, and their advantages and challenges.
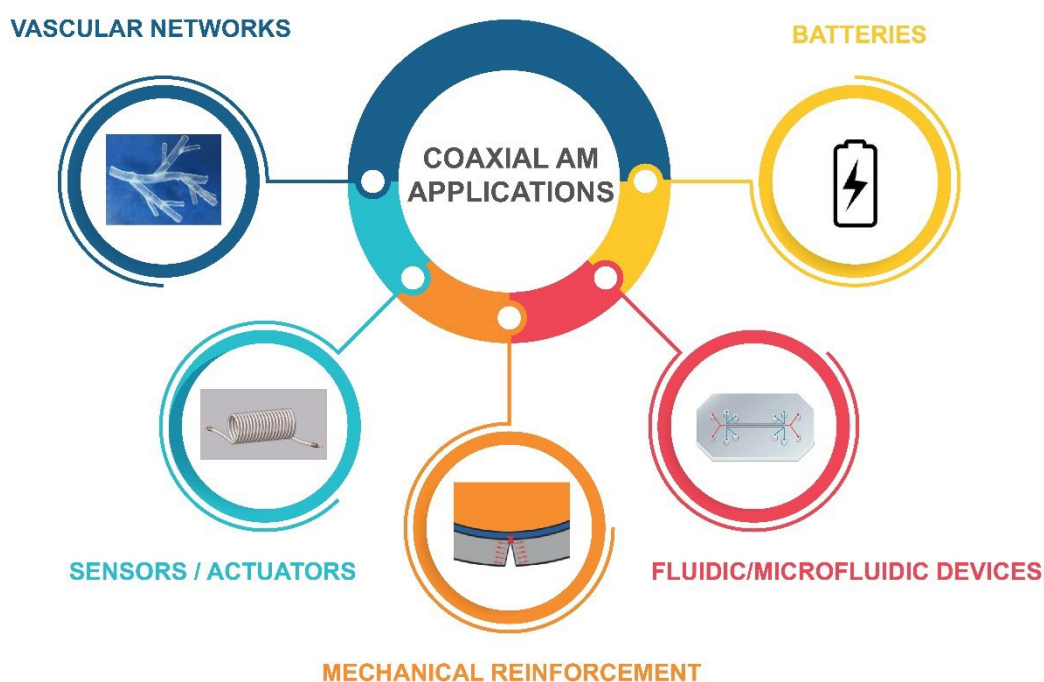
Figure 10. Some applications of coaxial AM including biomedical, fluidic and microfluidic devices, mechanical reinforcement, sensor and actuators, and batteries.

5.1 Biomedical

The role of coaxial additive manufacturing in biomedical applications is becoming more popular through its use in a variety of fields such as bioscaffolds, vascular networks, and fluidic and microfluidic devices. In coaxial biofabrication, two solutions of bio-ink and crosslinker are separately pushed through a coaxial nozzle, allowing the deposition of either a multimaterial bulk (inner needle bio-ink) or hollow fiber (bio-ink in the external needle) on the printing bed. Naturally derived polymers (e.g., gelatin [34], alginate [16,33,48,35,36,42–47], collagen [37,43,47–49], and silk fibroin [50]) and modified proteins [51] have been the most popular bio-inks processed into coaxial structures. The major challenge of such core–shell approach is that alginate fibers are hold together only by ionic crosslinked junctions that have scarce endurance in cell culture medium greatly limiting cell culture times.

5.1.1 Bio-scaffold fabrication

Bio compatible scaffolds provide the supporting structure for cell attachment and tissue development. One of the requirements of the scaffolds is to have a structural strength equivalent to the one of the native tissues. This strength requirement is particularly important for bone and articular cartilage where load bearing tissues exist. Development of coaxial struts could be a way to meet such a requirement by combining the mechanical properties of two or more materials. The outcome would be multimaterial composite struts that possess unique properties beyond a single material scaffold. For instance, multimaterial printing of scaffold would permit to attain simultaneously the desired mechanical and biomedical properties, which represent a

challenge when only one material is used. Cornock et al. [16] developed a coaxial additive manufacturing approach based on FFF to fabricate 2-3 layer square lattice core-sheath scaffolds characterized by a fiber diameter as small as 600μm, an offset as low as 60μm for the core material and a 200μm spacing between adjacent fibers. The scaffolds fabricated in their work were made of the alginate hydrogel and the thermoplastic polycaprolactone. The printed scaffolds met the strength requirements. Indeed, the ultimate stress of the scaffolds was as high as 2.8 ± 0.3 MPa for an elongation at break of $34 \pm 22\%$. Their modulus was equal 42 ± 9 MPa. Thus, these tensile tests showed that coaxial printed fibers are superior in strength and modulus compared to alginate hydrogels, making them excellent candidates for muscle and nerve repair. They work could also be used in the field of multi-phase release of therapeutics through the encapsulation of drugs within the 3D printed biocompatible macro-porous scaffolds.

Coaxial scaffold 3D printing using DIW technology was also reported in the literature [23,36,52]. Paredes et al. [23] presented a two-step method (see Figure 11**a**) for the 3D printing of core-sheath structured porous bio-scaffolds made of polymer and ceramics. Bioceramic scaffolds are particularly interesting in the field of bone tissue regeneration because they can guide the cellular mechanisms that naturally takes place in bone remodeling. In [23], the authors firstly employed DIW with coaxial nozzles for depositing beta-tricalcium phosphate bioscaffolds with hollow struts. Then, they filled the cores by suctioning polycaprolactone (PCL). The printed scaffold featured an external diameter d_e=1.08±0.03 mm, an internal diameter d_i=0.50±0.02 mm, a center-to-center spacing between struts s=2.00±0.08 mm, and layer height h=0.77±0.03 mm. SEM pictures of the coaxial and hollow printed scaffolds are shown in Figure 11**b**. The mechanical properties of the printed hybrid polymer/ceramic porous bioscaffolds were evaluated and compared to the ones of hollow and dense polymer scaffolds. The three types of scaffolds did not exhibit any significant differences in term of bending strength. However, the

compressive strength of the DIW scaffolds when the dense rods were replaced by hollow ones was substantially reduced. Polymer impregnation improved by more than 100% the compressive strength of the hybrid scaffolds compared to the hollow ones. In addition, in terms of strain energy density, that represents the toughness of the structure, the hybrid scaffolds revealed to be more than one order of magnitude more performant than hollow and dense scaffolds in bending. This work demonstrated that bioscaffolds that could mimic the mechanical performance of natural bones.
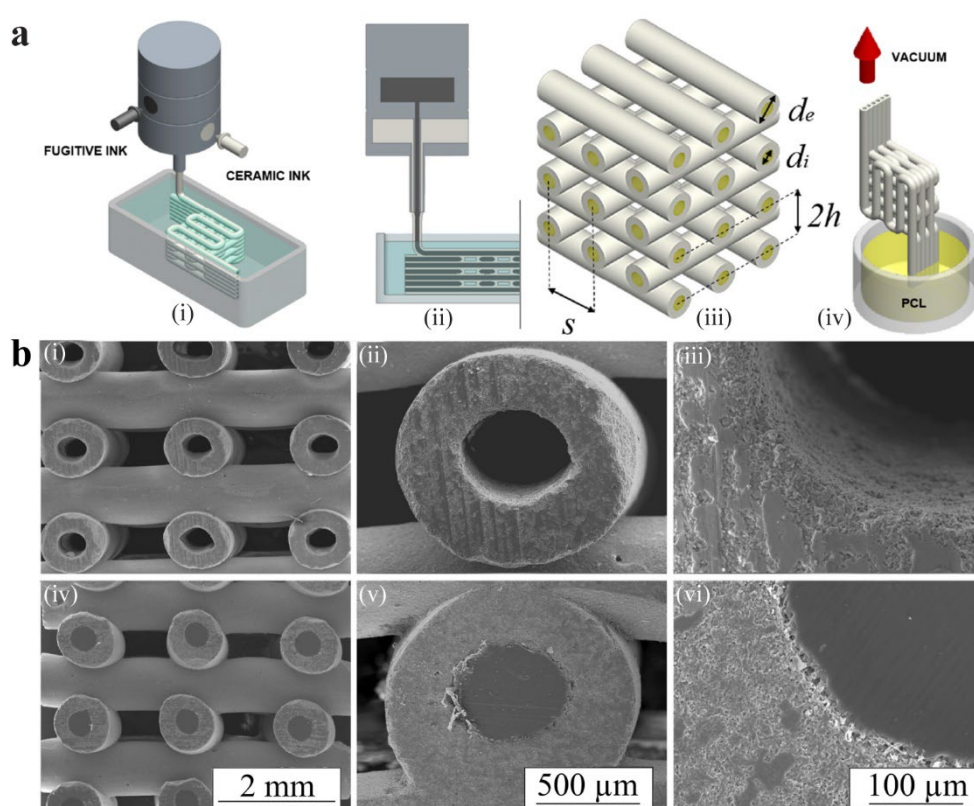

Figure 11. **a** (i-iv) co-extrusion of a bioceramic scaffold. The obtained structure was PCL-impregnated by vacuum suction as shown in (iv). **b** SEM micrographs at different magnifications of representative cross-sections of the scaffolds: (i-iii) hollow, (iv-vi) hybrid struts. Adapted with permission. [23] Copyright 2020, Elsevier.

Luo et al. [52] worked on 3D printed ceramic hollow bioscaffolds with macropores and multi-oriented hollow channel structures for bone regeneration enhancement. They used several nozzle sizes to build these bioscaffolds. After the scaffolds were printed, they were dried overnight at room temperature and then sintered at 1400°C for 3 h. Mechanical testing of the scaffolds showed that their properties were linked to their porosity which could be controlled by adjusting the diameter of the nozzles used in the printing process. The scaffolds demonstrated higher mechanical strength and stiffness (i.e. compressive strength of ~5 MPa and modulus of ~160 MPa) for the scaffold printed with the 16G/23G needle combination. These scaffolds also showed improved porosity and surface area for cell migration and new bone formation.

5.1.2   Vascular networks, fluidic and microfluidic applications

Many biomedical applications require tubular constructs or vascular-like structures [33,34,54,35,37,42–45,49,53]. Bioengineers choose to manufacture stand-alone tubes or complex perfusible constructions from bio-functional materials, or hydrogels, via fast and simple accessible routes.

Building such networks can be challenging due to the rather softness of hydrogel bioinks. As reported in the review of Ramezani et al. [55] coaxial bioprinting offers a solution to overcome this limitation as it allows the fabrication of complex vascularized tissue constructs, using sacrificial ink. A good illustration of the application of coaxial AM in the field of vascularized tissue constructs bioprinting is given in the work of Shao et al. [56] They successfully printed 10 mm sided cubes of vascularized tissue constructs using GelMa as the cell-laden bioink and gelatin as the sacrificial ink. The printed construct was then photo-crosslinked, cultured for 20 days before the sacrificial ink was removed. To demonstrate the effectiveness of the vascular network within the construct, the authors compared the cell viability within the construct with

and without vascular channels. They showed that the cell viability was higher in the vascularized construct than in the one without vascular channels and that the difference was more and more obvious as the culture time increased. To demonstrate the versatility of structures they could build using this coaxial bioprinting technique, Shao et al. manufactured more complex geometries like a 2D butterfly, an ear, a nose and a bone.

Mistry et al.[57] conducted a similar study, manufacturing formations of fibrous vascular-like cells using a cell-laden hydrogel as the core material and a partially crosslinked alginate or a hybrid hydrogel comprising alginate as the sheath material (characteristic size of ~800μm). The strands forming the structures were characterized by a mechanically robust shell and an extracellular matrix-mimicking core. The materials used not only improved the mechanical robustness of the structures compared to previous work, but also ensured the survival and function of encapsulated cells. Bioprinting could potentially be used to fabricate larger and more complex tissues on the basis of this work.

Millik et al. [37] reported a method wherein tailored coaxial nozzles were 3D printed using SLA 3D printers (see Figure 8**a**). Their custom-made nozzles could be used for the manufacture of hydrogel hollow structures through the co-extrusion of two shear-thinning hydrogels: a non-cross-linkable hydrogel playing the role of the sacrificial core material and a cross-linkable hydrogel used to print the tube walls. The authors fabricated tubes with various characteristics such as small diameters (<0.5 mm), various lengths (>15cm), wall thicknesses as small as ~150 μm and different cross-sectional shapes (e.g. circle, star). Following the coaxial DIW process, the printed coaxial fibers were cured with UV light (365 nm) to start the polymerization process and the cross-linking of the sheath hydrogel. The sacrificial core material was dissolved using water or a balanced salt solution (PBS) to therefore obtain the desired tubular structure. The inner and outer diameters of the tubes were measured at five different locations (~10 mm apart)

and appeared to be consistent along the length of the tubes. For the smaller-core tube, the measured inner diameter averaged 0.20±0.01 mm, and the outer diameter averaged 0.74±0.01 mm. Whereas for the larger-core tube, inner diameter averaged 0.43±0.01 mm, and the overall diameter averaged 0.70±0.01 mm. These measurements illustrate the high dimensional stability of the printed hollow tubes.

Liu et al. [34] developed a temperature-controlled multi-nozzle multi-channel deposition system (previously shown in Figure 7**c**) to create hollow tubes for a blood vessel made of gelatin-alginate and multicells. The multi-nozzle multi-channel deposition system has high and low temperature control units (set at 37°C and 4°C, respectively), for better solidification the blood vessel structure and control the appearance of a blood vessel. Microporous tubular bio-structures that can be used as blood vessels were successfully printed with this system, but clogging occured in the coaxial focusing nozzle on occasions.

3D vascular networks with multilevel fluidic channels made of hydrogel materials were 3D printed by Gao et al. [45]. The authors used macrochannels for mechanical stimulation and microchannels for the nutrient delivery and chemical stimulation. They extruded a biomaterial through coaxial nozzles illustrated in Figure 12**a**(i) and printed this coaxial structure around a rotating cylinder. The biomaterial they used was made of partially cross-linked hollow alginate fibers filled with fibroblast and smooth muscle cells. The main manufacturing steps are illustrated in Figure 12**a**. The hollow fibers they extruded were characterized by a diameter of 800-1500μm. These hollow filaments were 3D printed around a rotating cylinder of 2mm, 4mm, 6mm, or 8mm diameters. Then, endothelial cells were added into the tube. Optical and SEM pictures of the printed blood channels are shown in Figure 12**b**. Mechanical testing of the printed structure was then conducted. The results showed that the more the authors augmented the concentration of the sodium alginate in the biomaterial, the more the ultimate strength of

the printed structure increased (from 0.049±0.005 MPa in 2% alginate gels to 0.139±0.006 MPa in 3% alginate gels and 0.184±0.008 MPa in 4% alginate gels). Moreover, the authors demonstrated that the incubation time had a great influence on the mechanical properties of the structure. For 4% alginate gels, the ultimate strength decreased from 0.184±0.008 MPa to 0.145±0.011 MPa after two days, and decreased further to 0.105±0.003 MPa after five days. In addition, the biocompatibility of the printed channels was assessed by culturing them in a cell culture media (MEM) characterized by a 5% CO_2 atmosphere at 37 °C. The media was refreshed every couple days. The results of this experiment validated the biocompatibility of the channels, supporting the efficiency of their technique. The functional vascular networks printed are shown in Figure 12**c**. These vascular network configurations could be assimilated into organ-on-chip devices in order to create a better simulation of the microenvironment of blood vessels compared to previous vessel-on-chip models. However, the printing of very long vascular networks is still a challenge.
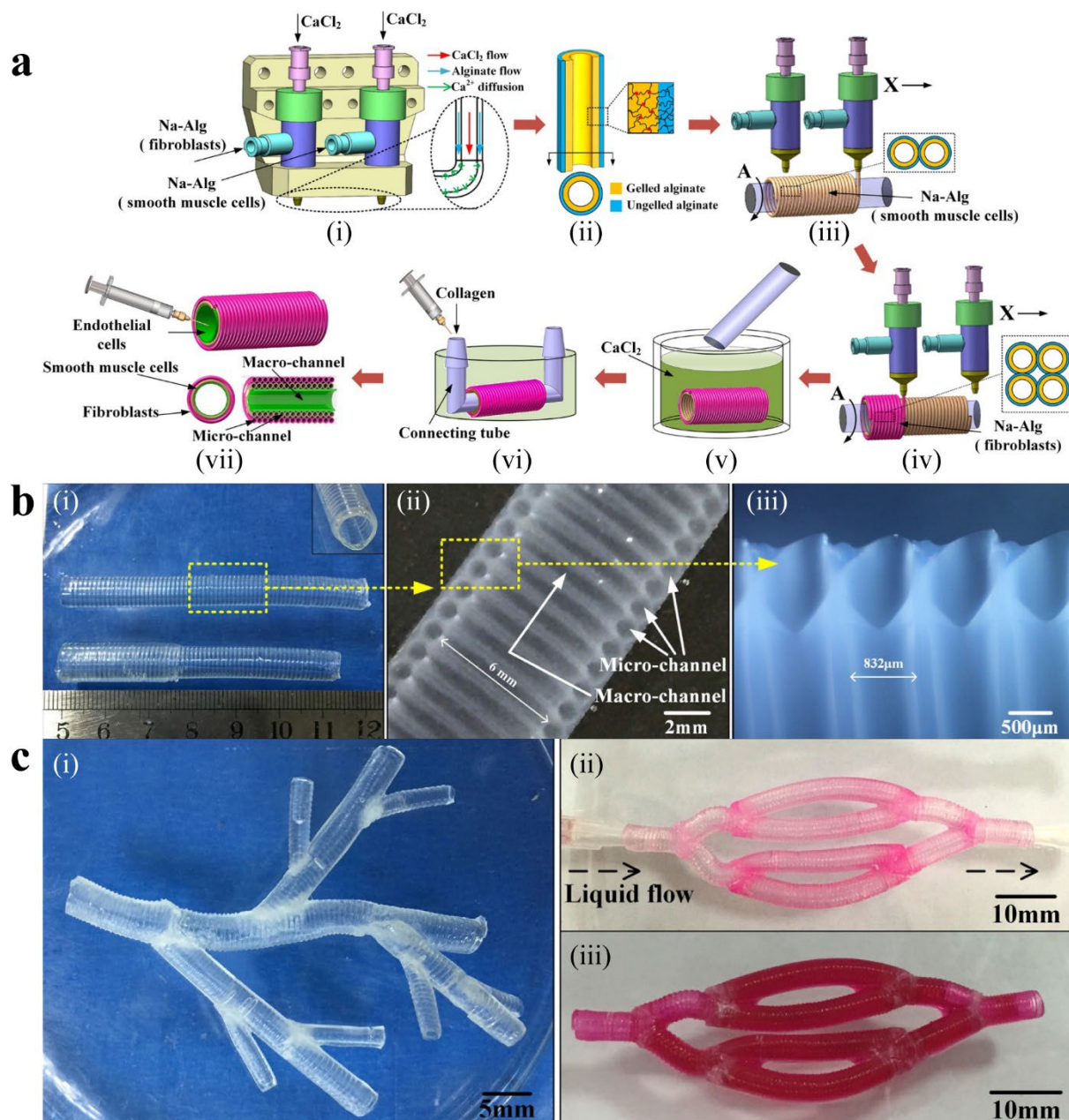
Figure 12. **a** manufacturing process of vascular alginate coil: (i) printing of hollow fibers, (ii) partial cross-linking of fibers, (iii) printing cell-laden tubes over a cylinder, (iv) creating a layer of fibroblasts-laden tubes over the previous one, (v) placing the fabricated tubular coil in CaCl$_2$ solution, (vi) ejection of collagen solution, (vii) passing endothelial cells into the coil; **b** morphology of the 3d printed vascular coil (i) optical image of a single-layer and a double-layer coil, (ii, iii) cross-sections and close up views. **c** Potential vascular network applications:

(i) vascular networks with branches, (ii) vascular circulation system, (iii) perfusion of cell culture media through the vascular circulation system. Adapted with permission. [45] Copyright 2020, American Chemical Society.

In another study, a freeform *in vitro* vascular model was constructed by Gao et al. [49] by directly printing a vessel and its support platform in a one-step fabrication process as illustrated in Figure 13**a**. They printed various designs including straight (Figure 13**b**(i)), curved (Figure 13**b**(ii)), serpentine (Figure 13**c**(iii)), dual-parallel, attached dual-curves, and discrete dual-curves patterns. All of these designs were characterized by a ~500μm channel diameter. The vascular models exhibited representative vascular functions such as selective permeability, antiplatelets/leukocytes adhesion, and self-remodeling in reaction to physiological shear stress and directional proangiogenic signals. The freeform, perfusable, and functional vascular models could be important devices to design different *in vitro* platforms. It could be used in a variety of biomedical applications, from modeling diseases related to blood vessel to fabrication of vascularized tissues and organs. One fundamental limitation of this approach is that the coaxial printing can only produce continuous tubes, making difficult the manufacture of models with branched vessels. However, a way to overcome this limitation would be to print multiple vessels in a single model and then fill the gaps using ECM hydrogels and cells.
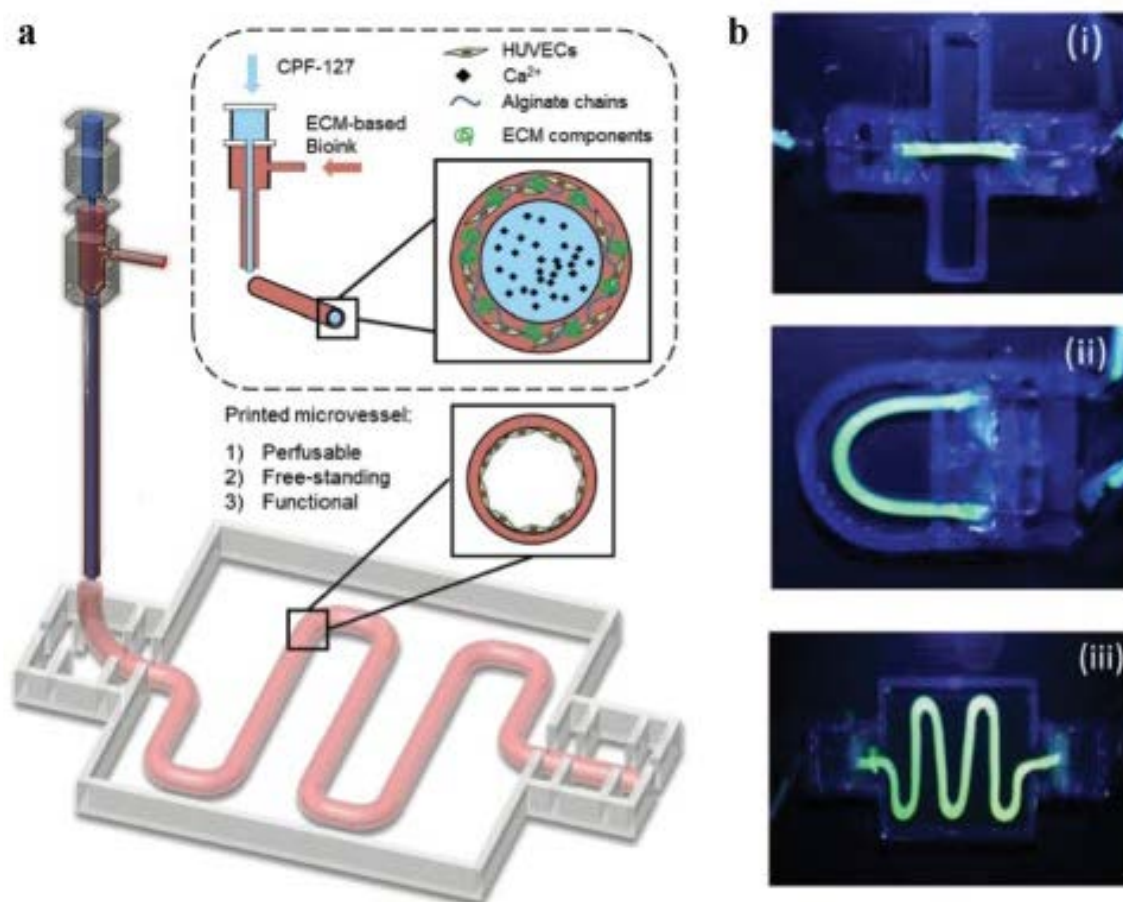
Figure 13. Fabrication of functional vascular models. **a** coaxial 3D printed vessels using human umbilical vein endothelial cells-laden vascular-tissue-derived extracellular matrix /alginate hybrid bioink; **b** perfused vascular models with straight, curved, and serpentine patterning designs. Reproduced with permission. [49] Copyright 2020, American Chemical Society.

Silva et al.[40] chose to follow a different approach to fabricate single-layered hollow tubular structures of different dimensions. Indeed, they focused their work on tri-material coaxial AM of vascular networks. They developed a triple-layered coaxial nozzle to be used in the biomanufacturing of vascular networks and vessels. Each of the three channels was used to extrude a different material. A support structure ink (methylcellulose-gelatin sacrificial ink) was extruded through the core channel whereas an alginate-based bioink and a $CaCl_2$ solution

flew through the center and the outer channels, respectively. They successfully printed single-layered hollow tubular structures and measured a cell viability above 80% in alginate-based hydrogels when the extrusion pressure was kept below 34 kPa. The advantage of using a triple-layered coaxial nozzle instead of a double-layered one is the potential of the nozzle to better mimic the complexity of human vascular networks in terms of histological and morphological characteristics of this vascular construct. Moreover, since the design of the nozzle allows the modification of the diameter of each channel, the wall thickness of a human blood vessel could be closely reproduced using such a device. Thus, a tripled-layer coaxial nozzle like the one presented in this study could be a viable solution to allow the biofabrication of a tissue-engineered blood vessel.

5.1.3 *Other biomedical applications*

Coaxial additive manufacturing has been also employed in cardiac tissue engineering to restore damaged tissues as well as establishing platforms for drug screening [46,47,51,58–62]. To this end, Zhu et al. [59] incorporated GelMA-coated gold nanorods (G-GNR) into a bioink based on gelatin methacryloyl (GelMA). The G-GNR/GelMA ink was made by integrating G-GNRs at different concentrations into a 7% GelMA prepolymer solution. A photo-initiator was then added to allow the covalent crosslinking of the ink. The more G-GNRs was added into the hydrogel, the more the electrical impedance was reduced. Moreover, the Young's modulus of the UV-cured hydrogel increased as G-GNRs were incorporated. These considerations led Zhu et al. to use G-GNR/GelMA hydrogels with a concentration of 0.1 and 0.25 mg.mL^{-1} characterized by a modulus of 4.2 ± 0.3 kPa and 4.7 ± 0.3 kPa, respectively, which are higher than the original GelMA hydrogel's modulus (3.75 ± 0.15 kPa). Even though the G-GNR/GelMA modulus was two orders of magnitude lower than the one of native human myocardium (425 ± 9 kPa), the authors speculated that the artificial construct could be

beneficial to the encapsulated cardiac cells by enabling their ordered contraction in the engineered tissues. Future works would allow the preparation of a solution that would potentially better mimic the mechanical properties of native tissues. The G-GNR/GelMA bioink and a $CaCl_2$ solution were then co-extruded using an Organovo bioprinter to build different types of constructs such as scaffolds or freeform spirals for instance. Cardiac cells showed enhanced cell adhesion and organization in the printed gold nanorod constructs compared to the ones fabricated without gold nanorods. Moreover, the the incorporation of gold nanorods allowed the filling of the electrically resistant pore walls of polymers, as well as the improvement of the coupling between cells and the promotion of synchronized contraction of the printed structures.

Liu et al. [51] used a coaxial bioprinting method to combine the benefits of both macro- and micro-encapsulation. The method consisted of the utilization of a tailored coaxial 3D printer and a bioink made of alginate-gelatin optimized for pancreatic islet encapsulation and 3D printing. Endothelial progenitor cells (EPC) have been successfully co-printed with pancreatic islets to produce 3D macroporous structures containing filaments that are in a coaxial configuration. The coaxial filament provided a protective shell layer and immunoprotection to the islets, which were positioned in the core. The platform they designed could improve the viability of islets after a transplantation and facilitate the surgical procedure. Their work is an important contribution towards new treatments for diseases such as Type I diabetes.

Peng et al.[63] also took advantage of coaxial AM to build a novel therapeutic method. Their objective was to build a self-adaptive all-in-one chip combining the different processes involved in skin wound therapy. The authors tried to combine these two objectives in a delivery chip that was coaxially 3D printed using a conductive hydrogel (graphene oxide-polypyrrole-alginate) solution anchored with proteins (chemokine) as the sheath material and an enzyme-inspired

gene delivery microcomplexes (crosslinked graphene oxide-polyethyleneimine) as the core material. Their proof-of-concept chip seemed to accelerate the wound closure and reduce the scarce compare to the blank control. This study paves the way for future innovations in the field of bio-inspired releasing systems aiming to achieve self-adaptive therapeutics delivery.

5.2 Flexible and stretchable sensors

Coaxial additive manufacturing was used to create flexible and stretchable sensors with, in some cases, a high degree of deformability and conformability in variety of applications such as wearable textiles, soft robotics, health tracking and human-machine interfaces [8].

An emerging way to build stretchable and or flexible devices is by using liquid metal alloys [10,28] or conductive fillers (e.g., silver paste [18], carbon-based conductive materials [6,8,11,15,50]). Liquid metals (LM) such as gallium-based liquid metal alloys with high conductivity have been used in flexible electronics. Two common gallium-based LM alloys are eutectic gallium indium (EGaIn) and Galinstan. EGaIn is an electrically conductive fluid metal and is composed of 75.5% Ga and 24.5% In by weight. The electrical conductivity of EGAIn is 3.4×10^6 S m^{-1} [64]. Galinstan represents a family of liquid metal eutectic mainly composed of gallium, indium, and tin. However, the most common form of Galinstan composed of 68wt% gallium, 22wt% of indium, and 10wt% of tin [64]. Both types of LM alloys exhibit similar physical properties.

5.2.1 Liquid metals

Alloys of liquid metals exhibit a high electrical conductivity and they are less toxic than traditional conductive materials such as mercury for instance. Various manufacturing techniques are being proposed to extrude liquid-metal alloy coaxially inside an enclosing sheath fluid to assure the stability and the continuity of the liquid metal flow. Using coaxial DIW 3D printing as shown in Figure 14 a conductive and stretchable cable with a core made of liquid

metal alloy (eutectic Gallium-Indium) and a PDMS sheath was developed in the work of Yan et al. [10]. To successfully DIW print such a cable, Yan et al. used the following printing parameters: the distance between the nozzle tip and the printing bed was set to less than 0.5 mm, the air pressures were fixed and the speed of the printing head was 10 mm/s. The printed coaxial cable was 20 mm long and the diameter of its core was ~0.24mm. Following the print (Figure 14**a**(i)), the cables were cured at 110°C for ~1 h in an incubator. Its two ends were then cut before inserting copper wires into the core of the cable, insuring a good contact with the liquid metal for electrical connection. Finally, the incisions were closed using drops of ultraviolet (UV) photosensitive resin as shown in Figure 14**a**(iii). Traction and compression mechanical tests of the cable was then conducted. The elastomeric matrix embedding the liquid metal exhibited a stretchability of over 35 folds. The cable also exhibited excellent cycling performance regarding its electrical properties when tested in tension as shown in Figure 14**c**(i). Moreover, during the compression tests (see Figure 14**c**(ii)), the manufactured cable demonstrated the capability to recover its original properties due to the high flowability of its core and the super elasticity of its shell.
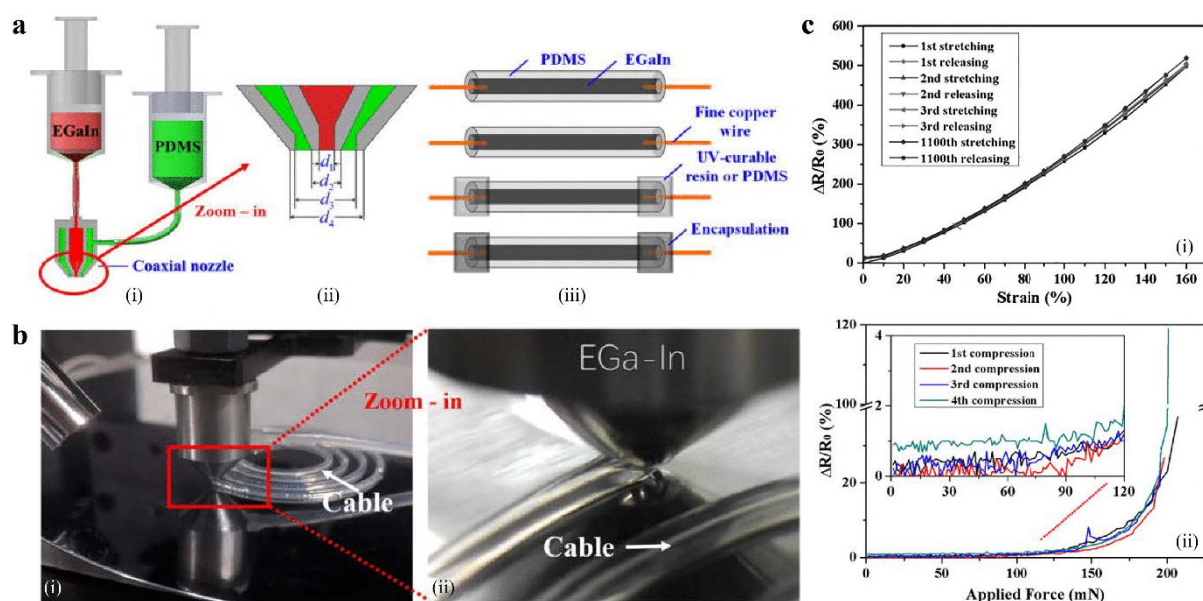
Figure 14 **a** coaxial printing of conductive cables (core diameter: 0.24 mm): (i-ii) coaxial design with EGaIn as the core and PDMS as the shell; (iii) fabrication steps from fine copper wire insertion to the reach of the the final device; **b** images of coaxial additive manufacturing process; **c** performance of fabricated cable: (i) cycling test results, (ii) compression test results. Adapted with permission. [10] Copyright 2016, AIP Publishing.

Zhou et al. [5] designed a 3D printed multifunction inductance flexible sensor made of silicone rubber and liquid metal (68.5% of Ga, 21.5% of In and 10% of Sn). A schematic of the device is shown in Figure 15**a**. By winding the coaxial tube into a spiral containing liquid metal during printing (see Figure 15**b**), the authors fabricated a solenoid-type inductor structure. This hollow cylinder structure made the sensor fit the shape of snake-like soft robots. The prototype of this sensor featured a length of 30 mm, a diameter of 9 mm, and 14 turns. The authors demonstrated the capability of this sensor by measuring tensile and bending deformations through the distinct variations of the inductance of the device. The setup used to evaluate the tensile and bending response of inductance sensors is shown in Figure 15**c**(i). Figure 15**c**(ii) represents the sensor inductance curve respect to the experimenter finger movements. The curvature measurements performed by the sensor were than compared to visual measurements and the maximum relative error was 7.96%.
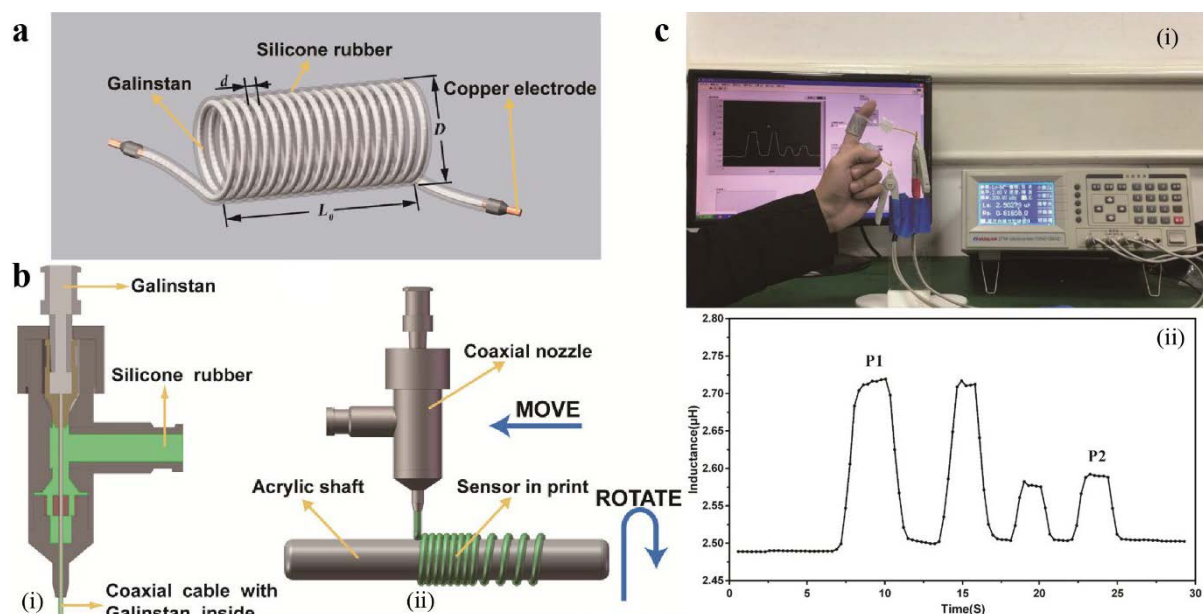
Figure 15. 3D printing of a coil-shaped flexible piezoresistive sensor: **a** isometric view of the sensor; **b** (i-ii) schematic of the coaxial nozzle and the 3D printing process; **c** (i) experimental setup of a figure curvature test, (ii) sensor inductance curve respect to different finger curvatures. Adapted with permission. [5] Copyright 2018, American Chemical Society.

Liquid metal (EGaIn) was also used in FFF processing of stretchable sensors but with a flexible thermoplastic matrix. A thermoplastic elastomer, poly (styrene-b-ethylene-co-butylene-b-styrene) (SEBS), was chosen by Khondoker et al. [28] (Figure 6**a**) because of its superior mechanical properties suitable for stretchable electronic applications. In their work, the authors used a commercially available type of SEBS, Kraton G1657 featuring very high elongation at break (~750%), relatively low modulus at 300% strain (2.4MPa), and high melt index (22 g/10 min at 230°C, 5 kg). The co-extruded liquid-metal core with SEBS insulating shell can be stretched up to four times its initial length without exhibiting any notable mechanical and electrical loss. Their study also showed no major effect on the average conductivity of liquid metal wire, which is about 3.67 x10^6 S/m.

Chen et al.[65] proposed a manufacturing process based on coaxial ink writing of continuous single core-shell fibers to fabricate conformable tactile sensors. Their process is made of four steps. Firstly, they printed a grid made of core-shell fibers using deionized water as the sacrificial material and PDMS as the elastomeric shell material. The fibers where characterized by a core diameter of ~400μm and a shell diameter of 1.5 mm. Secondly, they cured the structure by placing it in an oven at 80°C for 2h, causing the evaporation of the deionized water. Then, liquid metal (75,5% Gallium, 24,5% Indium) was injected in the core. Lastly, copper wires were inserted in each coaxial fiber and fixed using a UV photosensitive resin. The sensing device was then tested. Each fiber of the grid was connected in series with a 10 Ω resistance and to a voltage acquisition board CDAQ9174 and CDAQ9205 (National Instruments Ltd.) in parallel. A LabVIEW interface was developed to perform the data acquisition, the processing and the displaying of the sensing characterization results of the device. One sensing node was selected on the grid to do a repetitive compression test up to 1000 cycles. No resistance variation was measured in the top fiber when the force was less than 0.6N and in the bottom fiber when the force was less than 1.5N. Above these values, the resistance began to increase. The resistance variation ratio between the top and bottom fibers as the pressure changed showed good repeatability, allowing the definition of a relation between the applied pressure and the measured resistance. Moreover, the authors printed their sensing grids on a non-planar surface (ball) demonstrating the potential of their work in the field of soft robotics or human-machine interfacing.

5.2.2 *Carbon-based conductive nanomaterials*

Coaxial additive manufacturing technology was used for the fabrication of flexible fiber-shaped strain and pressure sensors [6–9,11]. Carbon-based conductive nanomaterials [66] such as carbon nanotubes (CNTs) [67–69], graphene nanoplatelets (GNPs) [67,68,70], graphene oxides (GO) [67,68,71],

and reduced-graphene oxide (rGO) [67,68] have been widely used for the creation of polymer matrix composites. The resolution of the printed parts is limited by the nozzle size being used for coaxial AM.

Gao et al. [11] demonstrated an integrated wearable sensor array fabricated with coaxial extrusion 3D-printing technology for simultaneously sensing pressure and the direction of external stimuli. In their study, the capacitive pressure sensor array was made of two layers of 3D printed electrodes, which were perpendicularly aligned. On top of the capacitive pressure sensor array, four resistance strain sensors printed in "U" shape with a gauge factor of 11.8 were assembled. The highest-pressure sensitivity the sensor could measure was 0.562 kPa^{-1}. Moreover, it had a relaxation speed of ~230 ms and a high detection limitation of 3 Pa. The integrated sensor also showed high durability making it suitable for applications in the field of electronic skins.

Tang et al. [8] developed a simple, adaptable and inexpensive coaxial additive manufacturing technique to print stretchable fibers for wearable strain sensors with a core-sheath configuration. Figure 16**a**(i) shows the fabrication of the insulating ink which is an extremely viscous silicone-modified elastomer solution, and the conductive ink which is a silicone elastomer solution comprising multi-walled CNTs. The insulating ink (sheath ink) was turned into printable ink by incorporating silica powders as viscosifiers. Figure 16**a**(ii-iii) illustrate the coaxial printing set up and the printed coaxial fiber, respectively. The machine used in this study was a custom-made 3D printing system, made of a simple computer-controlled 3-axis movement platform. The motion of the platform was coded by G-code commands produced by a slicer software according to the designed 3D models. The core and sheath inks were individually stored in two 20 mL pneumatic syringes. The appropriate pressure (i.e. 70 kPa and 640 kPa for core ink and sheath ink) was generated by an air compressor and controlled by two

pressure regulators to extrude both inks through the coaxial nozzle at a distance of 1.5 mm from the bed at a printing speed of 2 mm.s^{-1}. The printed co-axial fibers were then fully dried at 40 °C for 1 h in a oven. By changing the extrusion pressure of the inks, the dimensions of the printed coaxial fibers can flexibly be managed. Operation testing of the sensor showed that it can detect a strain of 0.1% with a stable response for over 15,000 cycles. As shown in Figure 16**b**, the sensor Tang et al. printed could detect and differentiate human joint movements. Furthermore, the printed sensors showed great waterproof performance, they were stretchable up to 150%, and they displayed outstanding sensitivities with gauge factors of 1.4 to 2.5 × 10^6.
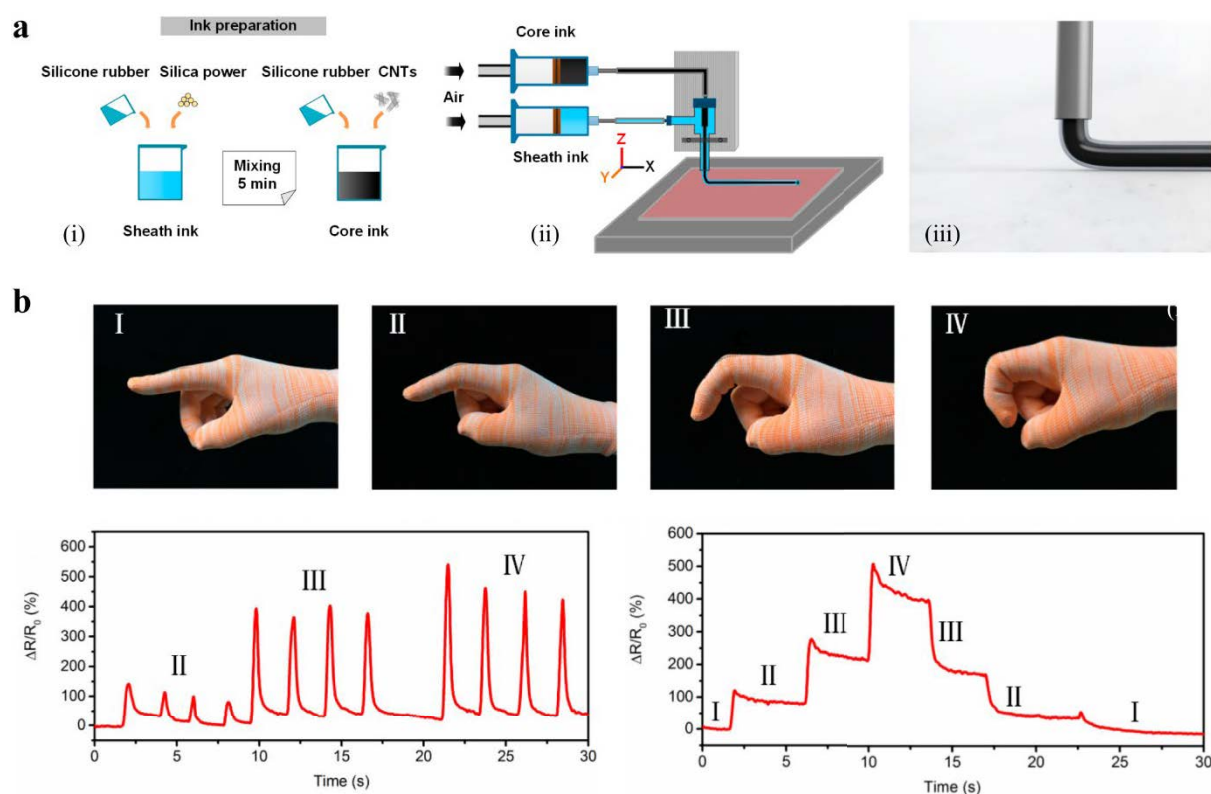

Figure 16 Core-shell fabrication of a flexible strain sensor: **a** (i) printable inks preparation, (ii) coaxial printing set-up, (ii) schematic of a printed fiber with coaxial structure; **b** (top) picture of the sensor woven into a glove in finger curvature test, (bottom left) relative resistance changes in bending/unbending motions of an index finger with various bending angles,

(bottom right) electrical resistance responses of the sensor under consecutive step-and-hold tests. Adapted with permission. [8] Copyright 2019, MDPI.

For high-performance micro and nanoelectromechanical systems (M/NEMS), controlled and meticulous patterning of nanostructures is vital. In a study performed by Wang et al. [7], a coaxial focused EHD jet printing technique was developed to create various nanostructures such as a nanowire array, a nano-freebeam and a nano-cantilever beam. Their technique was made of two steps: first, they printed the desired coaxial structure using a EHD jet printing set up then, the outer solution was removed to only keep the functional material as illustrated in Figure 17**a**. They designed and developed a coaxial needle technology, illustrated in Figure 17**a**(i-ii), in which the inner needle contains a practical ink, lead zirconate titanate (PZT), and outer needle contains a highly viscous liquid (silicon oil). Piezoceramics such as lead zirconate titanate (PZT) are important materials due to their electromechanical coupling. A robust coaxial jet was formed under optimized conditions of applied voltage, flow rate and needle-substrate distance (Figure 17**b**(i-iii)). Indeed, the external shearing force induces viscous shearing force and electrical field induces internal pressure, which was applied jointly to the internal functional ink, concentrating the nanoscale inner jet. This printing technique was used to manufacture nanostructures with closely aligned nanowire arrays, nano-free beams, and nano-cantilever beams down to a size of 40 nm. The needle used was 130 μm, and the needle size ratio over the printed structure size was as high as 3250/1. The nanostructures printed by PZT show significant piezoelectric performance [7].

Xu et al.[41] used a home-built coaxial direct ink writing system to fabricate smart elastomeric foam with embedded stretchable sensors. Carbon grease was used as the piezo-resistive core sensing material whereas PDMS was used as the elastomeric shell material. The foams were

manufactured according the following printing process: struts were printed using PDMS only extruded using a pressure of ~550 kPa; approaching the preset position of the embedded sensors, the purging pressure of the core material (~200 kPa) was switched on and the core ink started flowing simultaneously to the shell one. The printed structures were tested in compression and traction and their sensing performance was evaluated by measuring the electrical resistance variation of the core material as a function of the strain. The authors concluded that, the sensing struts should be subjecting to a stretching load rather than a compressive one for the achievement of a higher sensitivity.
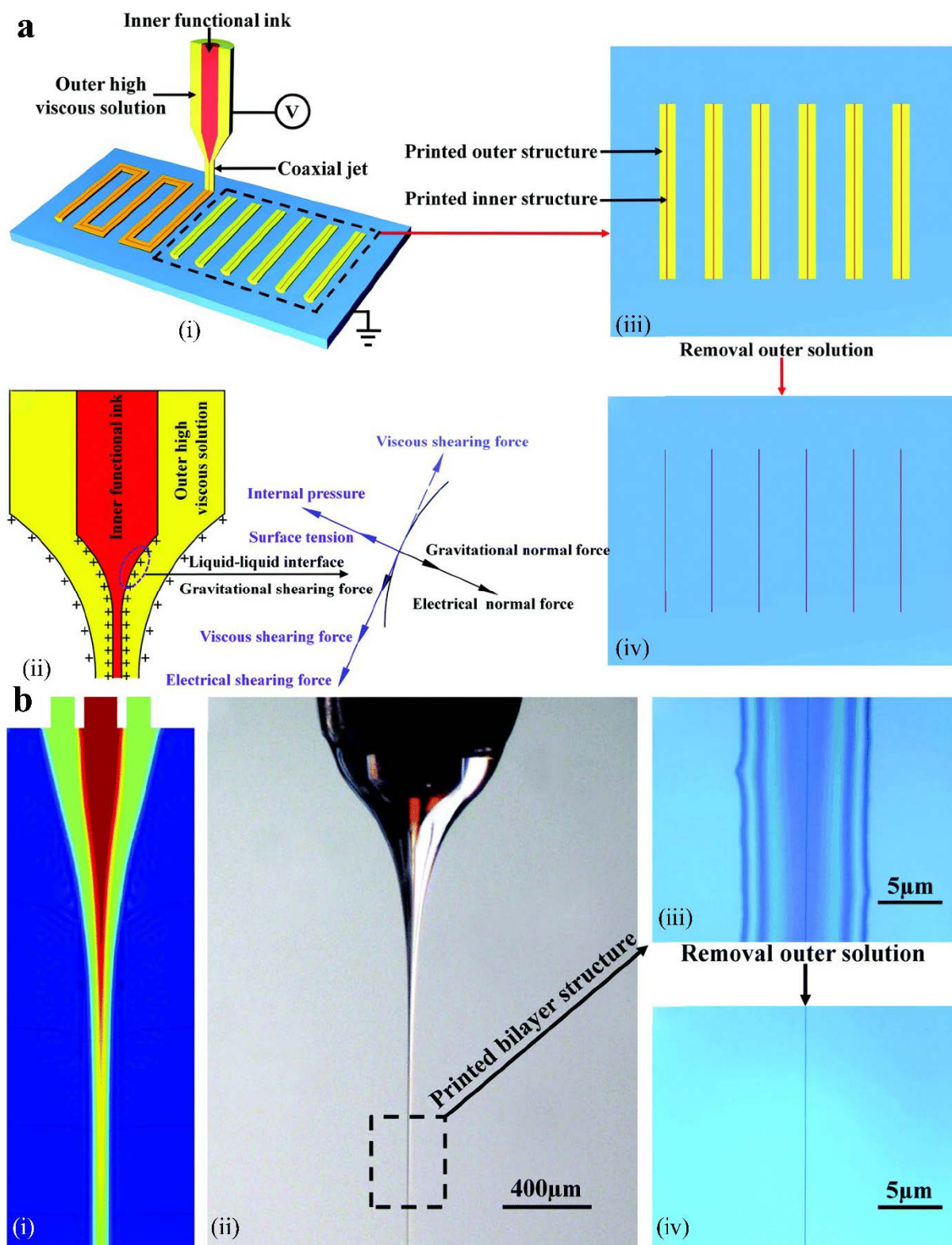
Figure 17 **a** (i) schematic of the coaxial jet printing process, (ii) graphical representation of

the forces in the coaxial jet (iii) schematic of printed coaxial structures (iv) representation of

the inner structure after removal of the outer material; **b** (i) simulation of the coaxial nozzle, (ii) optical image of the coaxial nozzle, (iii) 3D printed two-layer filament with the inner photoresist ink and outer layer silicone oil and, (iv) the inner photoresist ink after removing the silicone oil. Adapted with permission. [7] Copyright 2018, Royal Society of Chemistry.

5.2.3   *Piezoelectric materials*

Coaxial flexible piezoelectric sensors were also developed. For instance, Bodkhe et al. [18] used DIW to manufacture simultaneously piezoelectric sensors and their coextruded silver electrodes whereas conventional 3D printing of this kind of sensors usually involves a minimum of three steps (i.e. fabrication of the sensor structure, electrode deposition and electrical poling). In their work, they used an I&J 2200-4 (I&J Fisnar) robotic 3D printer to coextrude PVDF/BaTiO$_3$ nanocomposites with a commercially available silver ink in order to manufacture piezoelectric sensors. To demonstrate the 3D printability of such sensors, they printed a typical strain gauge shaped sensor on top of a FFF-printed part that had the shape of a dragonfly wing. When tested on an electromagnetic shaker for all the frequencies between 0.2 and 15 Hz, the sensor replicated the sinusoidal input very well. The authors then applied a sinusoidal input of 1 Hz to the wing. The response of the sensor to this input was a regular sine curve. Disturbances in the electrical output signal corresponding to physical obstructions and flow perturbations were also observed. All on these results demonstrated the applicability of the printed piezoelectric sensor for monitoring the aero-elastic behavior of the wing.

5.3   Coaxial actuators for soft robotics

Conventional robots are usually made of rigid parts built using materials like metals or rigid plastics whereas biological systems are fairly soft and stretchable. Based on this assessment,

there has been a rising interest for the use of softer materials in order to build robots that better mimic living organisms. To achieve that goal, researchers not only had to develop flexible and stretchable sensors like the one presented in the previous section (5.2), but they also had to find ways to manufacture soft actuators. Some of them decided to take advantage of coaxial AM to build such devices.

Chortos et al.[72] 3D printed core-sheath-shell dielectric elastomer fibers (DEF) and fiber bundles with programmable actuation. To print the sheath of their fibers, they elaborated a dielectric matrix ink made of Ecoflex silicone mixed with functionalized fumed silica. SE 1700 silicone was also added to obtain the required rheological behavior for printing. For the core and the shell of the fibers, they used a conductive ink made of an uncured silicone matrix (Eco30) mixed with hydrophobic carbon black. The authors 3D printed a multicore-shell nozzle using an Aureus Plus 3D printer and mounted it on an Aerotech 3-axis stage. They then printed core-sheath-shell fibers and fiber bundles using the conductive ink (core and shell) and the dielectric matrix ink (sheath). The printed devices were then cured following a three-step process (60°C for 24h followed by 80°C for 24h and 110°C for 24h). To assess the actuation behavior of the fibers, the authors clamped them onto a rectangular acrylic frame using alligator grips and they then applied an increasing voltage at a ramp rate of $100V.s^{-1}$ using a LabVIEW program. The deformation of the fibers was measured and the results were compared to an analytical model that predicted a quadratic dependence of strain with voltage. Up to 4% strain, the experiment results were consistent with the model. It is important to note that the axial actuation strain of the printed fibers of ≈10% is comparable to the largest strain reported in previous dielectric elastomer fibers. The authors also successfully printed vertical coil actuators and steerable DEF bundles.

5.4 E-textile

The textiles or fabrics with embedded digital components or electronics (also called E-textile), have the capacity to inherit characteristics of conventional fabrics such as softness, breathability and stretchability combined to the electronic features. Zhang et al. [50] developed a methodology for directly printing energy harvesting E-textile made of core-sheath fibers. Figure 18**a** illustrates this printed process in which two syringes filled with different inks (the core ink is a CNT aqueous solution and the sheath ink is a SF solution) were coupled to a coaxial spinneret, which was mounted on a 3D printer. Different feeding rates of CNT and SF inks were applied to form continuous core-sheath structured fibers despite the different cross-sectional areas of the inner and outer channels. The moving speed of the spinneret (i.e. 20 mm/s) was set to match the extruding rate of the core and the sheath inks (i.e. 10 mL/h and 25 mL/h, respectively). For various purposes, customer-designed or customized core-sheath fiber-based designs were easily printed on textiles without compromising the flexibility of fabric They printed a core-sheath fiber-based pattern by using CNTs as conductive-ink (core) and silk fiber (SF) as dielectric. This pattern was used as a textile triboelectric nanogenerator converting mechanical energy into electricity. The working principle of such a device is based on the coupling effect of contact electrification and electrostatic induction between the core-sheath fibers (Figure 18**b**). The authors printed some patterns on clothes to harvest body motion energy and provide a proof of concept of their work. Figure 18**c** shows schematic of a shirt with printed smart patterns at the underarms. The graph in Figure 18**c**(i) shows the typical alternating current generated by these patterns with a maximal short-circuit current (I_{sc}) peak 1.8 mA/cm^2. For concrete applications, a bridge rectifier was used to convert the alternating current to direct current using the electrical circuit illustrated in Figure 18**c**(ii). The graph in Figure 18**c**(iii) illustrates the corrected generated current. The biomechanical energy due to human body movement having a power

density up to 18mW/m² can be harvested by this E-textile. The authors also 3D printed a smart supercapacitor textile using a coaxial spinneret, which can be used for energy storage.

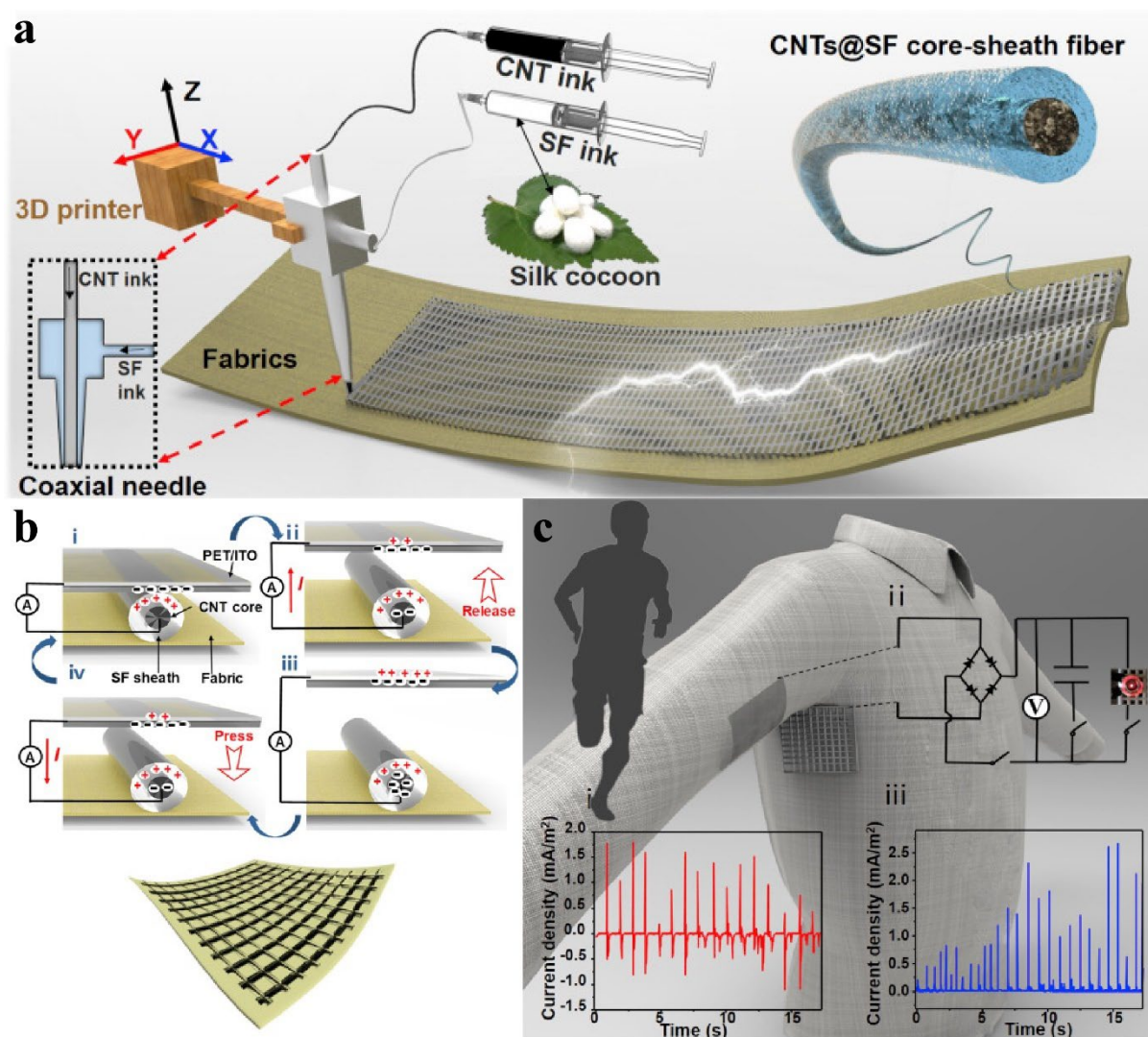

Figure 18. Coaxial core/shell 3d printing of fabrics. **a** schematic of the coaxial additive manufacturing process; **b** the working principle of the e-textile; **c** e-textile application: (i) output current density curve, (ii) rectifying circuit diagram of the power system, (iii) rectified output current density of the smart pattern. Adapted with permission. [50] Copyright 2019, Elsevier.

5.5 Batteries

A design (see Figure 6**b**(ii)) of flexible battery was suggested by Ragones et al. [30] and the initial outcomes of the production and characterization of 3D printed solid electrolytes prepared by FFF were reported. The multi-coaxial, cable-type 3D printed battery is one of the configurations with the possibility of a variety electrochemical energy sources. The battery design they proposed was made of 5 layers. From the center to the outer layer: the first layer acts as a current collector, the second one as an electrode, the third one as a solid electrolyte, the fourth one as another electrode and the last one as another current collector. Multi-coaxial, wire type battery structure makes ion transfer significantly easier by decreasing the twists and turns in the migration pathway in the battery being able to provide high power. In [30], the authors focused on the first step of the manufacture of such batteries which is the fabrication and characterization of the solid-state electrolytes. They made two solid polymer electrolytes containing LiTFSI (20% w/w), a lithium-ion conductor (20% w/w of PEO), polylactic acid (59% w/w of PLA) and ceramic fillers (1% w/w of SiO_2). The composite material obtained was extruded with a Felfil Evo Filament Extruder. The extruded filament had a 1.75 mm diameter circular cross section with a typical geometrical standard deviation of 0.02–0.03 mm which was suitable to be used as feedstock in an FFF 3D printer. To characterize the electrolytes, the authors printed a 19 mm diameter and 200 μm thick disc. The printed sample was placed between printed Lithium iron phosphate (LFP)-PLA and Lithium titanate (LTO)-PLA electrodes to prove the concept of all-solid-state printed battery. The cell was tested at 90°C. The cell's capacity only reached a few percent of the theoretical value and charge/discharge curves showed sloping profiles and low faradaic efficiency. Despite the modest performance of the cell, the authors provided a convincing demonstration of a solid battery printed by FFF. They are now working of the optimization of the composition and the fabrication of the

electrolytes as well as on the fabrication of a specially designed printing machine for multi-coaxial-cable battery. Even though they work is still at an early stage, it opens the way for the fabrication of multi-coaxial 3D-printed flexible cable battery of any shape.

5.6   Multi-layered architected lattices with tailored mechanical properties

Multi-coaxial 3D printing can enhance the mechanical properties of multi-layered architected lattices. In a study conducted by Mueller et al. [4], architected lattice structures made of core–shell struts characterized by high stiffness and toughness were printed (Figure 19). In order to achieve their goal, the authors used coaxial nozzles allowing the simultaneous extrusion of three materials: a flexible epoxy as the core material, a silicone as an interface material and a brittle epoxy as the shell material (Figure 19**a**). These nozzles were fabricated in a reproducible manner using SLA. Lattice structures, with and without elastomeric silicone interfacial layers were printed. Mechanical properties of the printed individual struts were assessed. Figure 19**b** illustrates the effects of different fillers on mechanical performance of these structures. The mechanical behavior of specimens made from the base resin is characterized by: an elastic modulus of 0.6 GPa, a tensile strength of 12 MPa, and an ultimate strain of 1.1. When fumed silica is added or the curing agent is increased, the stiffness and the strength of the struts are increased, whereas their fracture strain is reduced. On the other hand, the addition of rubber particles reduced the stiffness, the strength and the fracture strain of the struts. The authors produced an optimized flexible epoxy ink (characterized by a minimum rupture strain of 0.26, a high stiffness and strength of 1.25 GPa and 22 MPa, respectively) by optimizing the filler composition and relative ratios. Moreover, a three-point bending test was performed. Figure 19**c** shows the schematics and optical picture of the individual struts after the test. These pictures show that the strut remains partially intact. Indeed, the elastomeric interfacial layer diminishes the propagation of cracks from the brittle shell to the flexible core. Besides, the

representative load–displacement curves of the three-point bending test performed on individual struts of different composition and d/D ratios are given in Figure 19**d**. Figure 19**e** displays architected lattices printed by the authors using the tri-material coaxial AM technique. These lattices were tested in compression and the strain-stress curves of the structures are given in Figure 19**f**. During this test, the shells break into pieces while the core remains integral. By developing different printable materials and tailor-made coaxial nozzles, the authors were able to manufacture architected structured made of multicore–shell struts that concurrently possess high stiffness and toughness.
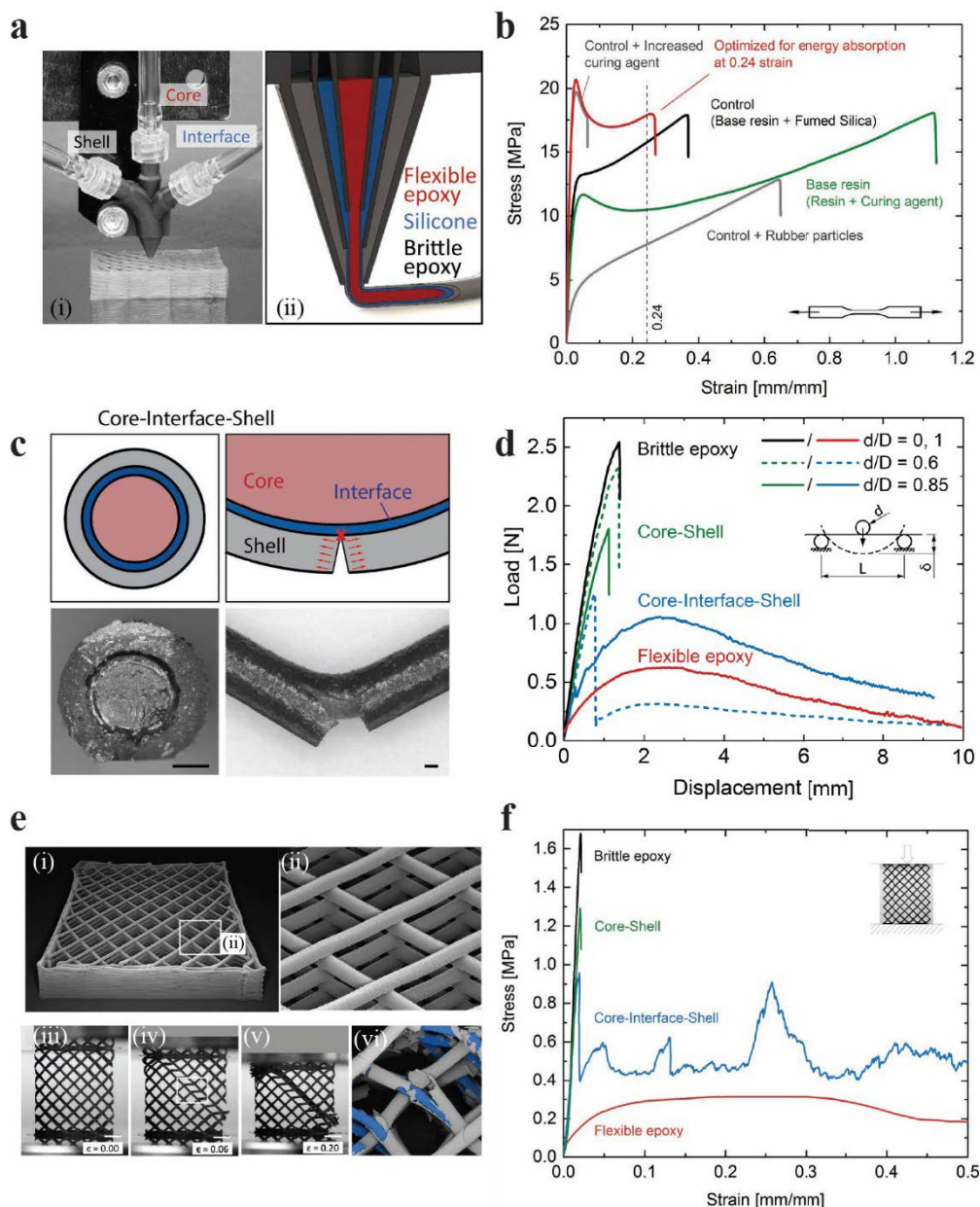
Figure 19. **a** multi-layer coaxial nozzle: (i) optical image of the nozzle, (ii) schematic of the cross-section; **b** tensile properties of the materials with different configurations; **c** schematic and optical pictures showing the elastomeric interfacial layer mitigates crack propagation from the brittle epoxy shell to the flexible epoxy core. [Scale bars = 200 μm]; **d** load–displacement response for representative struts of varying composition and inner diameter d /outer diameter D ratio; **e** architected lattices with core-interface-shell (CIS). (i–ii) lattice 3D printed by multi-core–shell DIW: (i) isometric view, (ii) struts close-up view, (iii)

compression tests that show a layer wise failure [scale bars = 8 mm]. iv-v) CIS lattice under compression, (vi) the interfacial layer stops crack propagation through the strut cores (false-colored blue), causing the shell to fracture into many pieces; **f** stress–strain curves for the previously shown CIS lattice compared with lattices composed of brittle epoxy, flexible epoxy, and C–S struts, as shown in (iv-v). Adapted with permission. [4] Copyright 2018, John Wiley and Sons.

6.   Conclusion and future directions

Coaxial additive manufacturing has evolved tremendously over the last decade as researchers found interest in the advantages of using this technique. Indeed, coaxial AM offers the possibility to combine the properties of different materials in a single-step process and thus, it allows the fabrication of more complex structures faster compared to traditional single-material AM techniques. It also allows to overcome the limitations of AM regarding the use of certain materials like liquid alloys through the use of enclosing sheath fluids. However, many of these fabrication techniques and applications are still at their early stages. Coaxial additive manufacturing faces challenges related to the interface and bonding between the inner and outer shells, optimization of printing parameters allowing the materials to flow continuously and synchronously and the difficulty to use solvent-based inks as the core material. Moreover, the printed resolution is limited by the nozzle geometry making difficult the fabrication of sub-micron-sized coaxial structures.

The most widely used technologies for coaxial additive manufacturing were DIW, EHD and FFF because those technologies can easily be adapted to print core-shell structures through the use of coaxial nozzles. Among these three currently applied techniques, DIW has evoked the

majority of interest due to its low cost, wide range of applicable materials, and ease of spatial and material deposition controllability.

A wide range of nozzle designs have been used in coaxial printing. While some of these coaxial nozzles were commercially available devices, others were custom-made and 3D printed using DLP, SLA, FFF or SLM for instance. The majority of the designed nozzles were made for DIW while the nozzles for FFF and EHD were limited to a few designs. Coaxial FFF nozzles for commercial dual extruders could benefit the 3D printing community in fabrication of creative and functional parts.

Coaxial additive manufacturing demonstrated to have various applications but the most common one lies in the area of in biomedicine. Coaxial DIW is successfully employed in variety of applications such as bio-fabrication, scaffold printing, and hydrogel tubes printing. However, the technology suffers from some limitations related to the almost unavoidable use of calcium-alginate hydrogels and the inherent characteristics of all extrusion-based printers. The inability to print very long vascular networks and the difficulty to create branched vascular structures in different ranges also represent important drawbacks of coaxial AM in this field of application.

Flexible sensors are another area of interest in core-shell 3D printing. Key limitations are shared with the characteristics of all extrusion-based and EHD 3D printers. For instance, the resolution is limited by the nozzle size for both categories of processes and also to the applied voltage for EHD. Thus, using coaxial AM to print submicron-sized structures is not yet possible.

The applications of coaxial additive manufacturing technology are broad and still emerging since the field is still in its early stages of development. Developing an optimum coaxial nozzle design for various coaxial additive manufacturing techniques, improving the quality and functionality of the printed parts and generalizing the use of coaxial AM to other fields of applications will certainly be the center points of future works. The process of bioprinting using

core–shell structure with combined biochemical and biomechanical properties represents a new strategy for fabricating functional human tissues and organs. In the design of electronic sensors over the next several years, we will most probably begin to see more innovative flexible sensors and energy storage devices following the growing investment and research of coaxial 3D printing. The other applications could be in 4D printing (four-dimensional printing where time is the fourth dimension) for the creation of multimaterial coaxial structures that could change their shape under the influence of external stimuli such as heat or light for instance.

Acknowledgements

Received: ((will be filled in by the editorial staff))

Revised: ((will be filled in by the editorial staff))

Published online: ((will be filled in by the editorial staff))

References

[1]   M. Rafiee, R. D. Farahani, D. Therriault, *Adv. Sci.* **2020**, *7*, 1902307.

[2]   M. Costantini, C. Colosi, W. Święszkowski, A. Barbetta, *Biofabrication* **2019**, *11*, DOI 10.1088/1758-5090/aae605.

[3]   Z. Yin, Y. Huang, Y. Duan, H. Zhang, *Electrohydrodynamic Direct-Writing for Flexible Electronic Manufacturing*, **2017**.

[4]   J. Mueller, J. R. Raney, K. Shea, J. A. Lewis, *Adv. Mater.* **2018**, *1705001*, 1.

[5]   L. Y. Zhou, Q. Gao, J. F. Zhan, C. Q. Xie, J. Z. Fu, Y. He, *ACS Appl. Mater. Interfaces* **2018**, *10*, 23208.

[6]   Z. Tang, S. Jia, F. Wang, C. Bian, Y. Chen, Y. Wang, B. Li, *ACS Appl. Mater. Interfaces* **2018**, *10*, 6624−6635.

[7]   D. Wang, X. Zhao, Y. Lin, J. Liang, T. Ren, Z. Liuc, J. Li, *Nanoscale* **2018**, *10*, 9867.

[8]   Z. Tang, S. Jia, X. Shi, B. Li, C. Zhou, *Polymers (Basel).* **2019**, *11*, 666.

[9]   Q. Xu, S. W. R. Lee, J. C. C. Lo, *EMAP 2018 - 2018 20th Int. Conf. Electron. Mater. Packag.* **2019**, 1.

[10]   H. L. Yan, Y. Q. Chen, Y. Q. Deng, L. L. Zhang, X. Hong, W. M. Lau, J. Mei, D. Hui, H. Yan, Y. Liu, *Appl. Phys. Lett.* **2016**, *109*, 1.

[11]   Y. Gao, G. Yu, T. Shu, Y. Chen, W. Yang, Y. Liu, J. Long, W. Xiong, F. Xuan, *Adv. Mater. Technol.* **2019**, *4*, 1.

[12]   W. C. Yan, Y. W. Tong, C. H. Wang, *AIChE J.* **2017**, *63*, 5303.

[13]   A. C. Taylor, S. Beirne, G. Alici, G. G. Wallace, *Rapid Prototyp. J.* **2017**, *23*, 543.

[14]   B. Wang, X. Chen, Z. Ahmad, J. Huang, M. W. Chang, *Adv. Eng. Mater.* **2019**, *21*, 1.

[15]   R. Cornock, S. Beirne, G. G. Wallace, in *2013 IEEE/ASME Int. Conf. Adv. Intell. Mechatronics Mechatronics Hum. Wellbeing, AIM 2013*, IEEE, **2013**, pp. 973–978.

[16] R. Cornock, B Thompson, G. G. Wallace, *Biofabrication* **2014**, *6*, 025002.

[17] A. Afzal, J. Y. Drean, O. Harzallah, N. Khenoussi, S. Ahmad, N. A. Akhtar, *Text. Res. J.* **2017**, *87*, 1991.

[18] S. Bodkhe, C. Noonan, F. P. Gosselin, D. Therriault, *Adv. Eng. Mater.* **2018**, *20*, 1.

[19] D. Zindani, K. Kumar, *Int. J. Light. Mater. Manuf.* **2019**, *2*, 267.

[20] P. K., M. M., S. P. P., *Curr. Opin. Chem. Eng.* **2020**, *28*, 51.

[21] R. D. Farahani, K. Chizari, D. Therriault, *Nanoscale* **2014**, *6*, 10470.

[22] E. D. Elia, N. Ni, M. Sha, E. Saiz, *ACS Appl. Mater. Interfaces* **2017**, *9*, 37136.

[23] C. Paredes, F. J. Martínez-Vázquez, A. Pajares, P. Miranda, *Ceram. Int.* **2019**, *45*, 19572.

[24] N. W. Solís Pinargote, A. Smirnov, N. Peretyagin, A. Seleznev, P. Peretyagin, *Nanomaterials* **2020**, *10*, 1300.

[25] C. Portet, P. L. Taberna, P. Simon, C. Laberty-Robert, *Electrochim. Acta* **2004**, *49*, 905.

[26] I. Gibson, D. Rosen, B. Stucker, *Additive Manufacturing Technologies: 3D Printing, Rapid Prototyping, and Direct Digital Manufacturing*, Springer, **2015**.

[27] J. Anu Bhushani, C. Anandharamakrishnan, *Trends Food Sci. Technol.* **2014**, *38*, 21.

[28] M. A. H. Khondoker, A. Ostashek, D. Sameoto, *Adv. Eng. Mater.* **2019**, *21*, 1900060.

[29] M. A. H. Khondoker, A. Asad, D. Sameoto, *Rapid Prototyp. J.* **2018**, *24*, 921.

[30] H. Ragones, A. Vinegrad, G. Ardel, M. Goor, Y. Kamir, M. M. Dorfman, A. Gladkikh, D. Golodnitsky, *J. Electrochem. Soc.* **2020**, *167*, 070503.

[31] S. Duchi, C. Onofrillo, C. D. O'Connell, R. Blanchard, C. Augustine, A. F. Quigley, R. M. I. Kapsa, P. Pivonka, G. Wallace, C. Di Bella, P. F. M. Choong, *Sci. Rep.* **2017**, *7*, 1.

[32] C. D. O'Connell, C. Di Bella, F. Thompson, C. Augustine, S. Beirne, R. Cornock, C. J. Richards, J. Chung, S. Gambhir, Z. Yue, J. Bourke, B. Zhang, A. Taylor, A. Quigley, R. Kapsa, P. Choong, G. G. Wallace, *Biofabrication* **2016**, *8*, DOI 10.1088/1758-5090/8/1/015019.

[33] Q. Gao, Y. He, J. zhong Fu, A. Liu, L. Ma, *Biomaterials* **2015**, *61*, 203.

[34] H. Liu, H. Zhou, H. Lan, F. Liu, X. Wang, *SLAS Technol.* **2018**, *23*, 64.

[35] Y. Li, Y. Liu, C. Jiang, S. Li, G. Liang, Q. Hu, *Soft Matter* **2016**, *12*, 2392.

[36] C. Colosi, M. Costantini, R. Latini, S. Ciccarelli, A. Stampella, A. Barbetta, M. Massimi, C. Devirgiliis, *J. Mater. Chem.* **2014**, *2*, 6779.

[37] S. C. Millik, A. M. Dostie, D. G. Karis, P. T. Smith, M. McKenna, N. Chan, C. D. Curtis, E. Nance, A. B. Theberge, A. Nelson, *Biofabrication* **2019**, *11*, 045009.

[38] K. Alessandri, M. Feyeux, B. Gurchenkov, C. Delgado, A. Trushko, K.-H. Krause, D. Vignjević, P. Nassoy, A. Roux, *Lab Chip* **2016**, *16*, 1593.

[39] Y. Jin, D. Zhao, Y. Huang, *J. Micro Nano-Manufacturing* **2017**, *5*, 1.

[40] C. Silva, C. J. Cortés-Rodriguez, J. Hazur, S. Reakasame, A. R. Boccaccini, *Int. J. Bioprinting* **2020**, *6*, 1.

[41] J. Xu, X. Zhang, Y. Liu, Y. Zhang, H. Y. Nie, G. Zhang, W. Gao, *Addit. Manuf.* **2020**, *36*, 101487.

[42] R. Attalla, P. R. Selvaganapathy, *18th Int. Conf. Miniaturized Syst. Chem. Life Sci. MicroTAS 2014* **2014**, 479.

[43] G. Gao, J. H. Lee, J. Jang, D. H. Lee, J. Kong, B. S. Kim, *Tissue Eng.* **2017**, *1700798*, 1.

[44] R. Attalla, C. Ling, P. Selvaganapathy, *Biomed Microdevices* **2016**, *18*, 17.

[45] Q. Gao, Z. Liu, Z. Lin, J. Qiu, Y. Liu, A. Liu, Y. Wang, M. Xiang, B. Chen, J. Fu, Y.

He, *acs biom* **2017**, *3*, 2.

[46] Y. Zhou, S. Liao, X. Tao, X. Xu, Q. Hong, D. Wu, Y. Wang, *ACS Appl. Bio Mater.* **2018**, *1*, 502−510.

[47] J. He, J. Shao, X. Li, Q. Huang, T. Xu, *Bioprinting* **2018**, *11*, 1.

[48] Y. Yu, K. K. Moncal, J. Li, W. Peng, I. Rivero, J. A. Martin, I. T. Ozbolat, *Sci. Rep.* **2016**, *6*, 28714.

[49] G. Gao, J. Y. Park, B. S. Kim, J. Jang, D. Cho, *Adv. Healthc. Mater.* **2018**, *1801102*, 1.

[50] M. Zhang, M. Zhao, M. Jian, C. Wang, A. Yu, Z. Yin, X. Liang, H. Wang, K. Xia, X. Liang, J. Zhai, Y. Zhang, *Matter* **2019**, *1*, 1.

[51] X. Liu, S. D. Carter, M. J. Renes, J. Kim, D. M. Rojas-canales, D. Penko, C. Angus, S. Beirne, C. J. Drogemuller, Z. Yue, P. T. Coates, G. G. Wallace, *Adv. Healthc. Mater.* **2019**, *1801181*, 1.

[52] Y. Luo, D. Zhai, Z. Huan, H. Zhu, L. Xia, J. Chang, C. Wu, *ACS Appl. Mater. Interfaces* **2015**, *7*, 24377−24383.

[53] Y. Zhang, H. Chen, I. T. Ozbolat, in *Proc. ASME 2012 Int. Mech. Eng. Congr. Expo. IMECE2012*, **2012**, pp. 1–6.

[54] i P. N. and A. R. Kevin Alessandri,‡abc Maxime Feyeux,‡d Basile Gurchenkov, bcghi Christophe Delgado, d Anastasiya Trushko, a Karl-Heinz Krause, d Daniela Vignjević, i Pierre Nassoyabef and Aurélien RouxKevin Alessandri,‡abc Maxime Feyeux,‡d Basile Gurchenkov, bcghi Christ, K. Alessandri, M. Feyeux, B. Gurchenkov, C. Delgado, A. Trushko, K.-H. Krause, D. Vignjević, P. Nassoy, A. Roux, *Lab Chip* **2016**, *16*, 1593.

[55] H. Ramezani, L. yu Zhou, L. Shao, Y. He, *J. Zhejiang Univ. Sci. A* **2020**, *21*, 859.

[56] L. Shao, Q. Gao, C. Xie, J. Fu, M. Xiang, Y. He, *Biofabrication* **2020**, *12*, DOI

10.1088/1758-5090/ab7e76.

[57]   P. Mistry, A. Aied, M. Alexander, K. Shakesheff, A. Bennett, J. Yang, *Macromol. Biosci.* **2017**, *17*, 1.

[58]   H. Liang, J. He, J. Chang, B. Zhang, D. Li, *Int. J. Bioprinting* **2017**, *4*, 1.

[59]   K. Zhu, S. R. Shin, T. Van Kempen, Y. Li, V. Ponraj, A. Nasajpour, S. Mandla, N. Hu, X. Liu, J. Leijten, Y. Lin, M. A. Hussain, Y. S. Zhang, A. Tamayol, A. Khademhosseini, *Adv. Funct. Mater.* **2017**, *27*, 1605352.

[60]   W. Mao, M. K. Kang, J. U. Shin, Y. J. Son, H. S. Kim, H. S. Yoo, *ACS Appl. Mater. Interfaces* **2018**, *10*, 43503.

[61]   2 Baolin Wang1, M.-W. C. , Xing Chen1, 2* Zeeshan Ahmad3 , Jie Huang4, **2019**, DOI 10.1002/adem.201900699.

[62]   P. Jiang, C. Yan, Y. Guo, X. Zhang, M. Cai, X. Jia, X. Wang, F. Zhou, *Biomater. Sci.* **2019**, *7*, 1805.

[63]   L. H. Peng, X. H. Xu, Y. F. Huang, X. L. Zhao, B. Zhao, S. Y. Cai, M. J. Xie, M. Z. Wang, T. J. Yuan, Y. He, Z. Xu, J. Q. Gao, C. Gao, *Adv. Funct. Mater.* **2020**, *30*, 1.

[64]   S. Cheng, Z. Wu, *Lab Chip* **2012**, *12*, 2782.

[65]   Y. Chen, Y. Liu, J. Ren, W. Yang, E. Shang, K. Ma, L. Zhang, J. Jiang, X. Sun, *Mater. Des.* **2020**, *190*, 108567.

[66]   M. Rafiee, Modeling, Processing, Fabrication and Characterization of Carbon Nanomaterials-Reinforced Polymer Composites, **2018**.

[67]   M. Rafiee, F. Nitzsche, J. Laliberte, S. Hind, F. Robitaille, M. R. Labrosse, *Compos. Part B Eng.* **2019**, *164*, 1.

[68]   M. Rafiee, F. Nitzsche, J. Laliberte, J. Thibault, M. Labrosse, *Polym. Compos.* **2019**, *40*, E1732.

[69]   M. Rafiee, F. Nitzsche, M. R. Labrosse, *Polym. Test.* **2018**, *69*, 385.

[70]   M. Rafiee, F. Nitzsche, M. R. Labrosse, *Polym. Compos.* **2019**, *40*, 3914.

[71]   M. Rafiee, F. Nitzsche, M. R. Labrosse, *J. Compos. Mater.* **2019**, *53*, 2105.

[72]   A. Chortos, J. Mao, J. Mueller, E. Hajiesmaili, J. A. Lewis, D. R. Clarke, *Adv. Funct. Mater.* **2021**, *2010643*, 1.

Biography of Dr. Mohammad Rafiee

Mohammad Rafiee received his Ph.D. degree in Mechanical Engineering from the University of Ottawa. Currently, he is a Postdoctoral Fellow at National Research Council Canada. His research interests are focused on the development of advanced materials, smart devices and additive manufacturing. He has developed innovative materials and structures with new functionalities.

Biography of Floriane Granier

Floriane Granier is a Master's student in the aerospace engineering department at Polytechnique Montreal. Her research focuses on the development of advanced materials for multi-material, multi-process additive manufacturing of self-sensing and energy harvesting devices.

Biography of Prof. Daniel Therriault

Daniel Therriault is a full professor in the Mechanical Engineering Department at Polytechnique Montreal. He currently holds two Chairs: a Canada Research Chair on the fabrication of advanced microsystems and materials, and the Safran-Polytechnique Industrial Chair on the additive manufacturing of reinforced polymers. He is co-director of the Laboratory for Multiscale Mechanics (LM2). His research interests are related to additive manufacturing of advanced materials and multifunctional composites for aerospace applications, and for biomedical and microsystems.

Coaxial additive manufacturing is particularly attractive due to its unique feature of simultaneously depositing two or more materials with a common axis. This feature benefits various fields from biomedical and tissue engineering to electronics and composites. The present work compares coaxial additive manufacturing technologies, discusses the advantages and disadvantages and provides future directions.

Mohammad Rafiee, Floriane Granier, and Daniel Therriault

Advances in coaxial additive manufacturing and applications